CHAPTER 12: COMBINED APATITE FISSION TRACK AND U–Pb DATING BY LA–ICP–MS AND ITS APPLICATION IN APATITE PROVENANCE ANALYSIS

David M. Chew
Department of Geology, School of Natural Sciences,
Trinity College Dublin,
Dublin 2, Ireland
chewd@tcd.ie

and

Raymond A. Donelick
Apatite to Zircon, Inc.,
1075 Matson Road,
Viola, Idaho 83872-9709, U.S.A.
donelick@apatite.com

INTRODUCTION

Apatite is a common accessory mineral in igneous, metamorphic and clastic sedimentary rocks. It is a nearly ubiquitous accessory phase in igneous rocks, due in part to the low solubility of P_2O_5 in silicate melts and the limited amount of phosphorus incorporated into the crystal lattices of the major rock-forming minerals (Piccoli & Candela 2002). Apatite is common in metamorphic rocks of pelitic, carbonate, basaltic, and ultramafic composition and is found at all metamorphic grades from transitional diagenetic environments to migmatite (Spear & Pyle 2002). Apatite is also virtually ubiquitous in clastic sedimentary rocks (Morton & Hallsworth 1999).

Apatite is widely employed in low temperature thermochronology studies with the apatite fission track and apatite (U–Th)/He thermochronometers yielding thermal history information in the 60–110°C (Laslett *et al.* 1987) and 55–80°C (Farley 2000) temperature windows, respectively. Apatite has also been employed in high temperature thermochronology studies, which demonstrate that the U–Pb apatite system has a closure temperature of ca. 450–550°C (Chamberlain & Bowring 2000, Schoene & Bowring 2007). Apatite has also been employed in Lu–Hf geochronology studies (Barfod *et al.* 2003) and as an Nd isotopic tracer (Foster & Vance 2006, Gregory *et al.* 2009).

Detrital apatite analysis has many potential applications in sedimentary provenance studies. Detrital thermochronology is a provenance tool which deciphers the thermotectonic history of source regions (typically orogenic belts) by studying the chronology of their erosional products. To date, the majority of apatite provenance studies have focused on detrital thermochronology of apatite using the fission track or (U–Th)/He thermochronometers (*e.g.*, Bernet & Spiegel 2004). Apatite can incorporate nearly half of the elements in the periodic table in its crystal structure and many trace elements in apatite display a large range of concentrations. Unlike zircon, the trace element partition coefficients in igneous apatite are typically very sensitive to changes in magmatic conditions (Sha & Chappell 1999) and therefore the trace element chemistry of detrital apatite provides a link to the parent igneous rock type in provenance studies (Jennings *et al.* 2011).

Zircon provenance studies have been revolutionized in the last decade by the advent of the LA–ICP–MS U–Pb method, which offers low cost, rapid data acquisition and sample throughput compared to the ID–TIMS or ion microprobe U–Pb methods (*e.g.*, Košler & Sylvester 2003). LA–ICP–MS U–Pb dating of apatite is more challenging as apatite typically yields lower U and Pb concentrations and higher common Pb to radiogenic Pb ratios which nearly always necessitate common Pb correction. In contrast to the well documented polycyclic behavior of the stable heavy mineral zircon, apatite is unstable in acidic groundwater and weathering profiles and has only limited mechanical stability in sedimentary transport systems (Morton & Hallsworth 1999). It therefore more likely represents first cycle detritus, and hence U–Pb apatite dating would yield complementary information to U–Pb zircon provenance studies.

Fission track and U–Pb dating are therefore two of the most useful (and most rapid) techniques in

Mineralogical Association of Canada Short Course 42, St. John's NL, May 2012, p. 219-247

apatite provenance studies. They yield complementary information, with the apatite fission track system yielding low-temperature exhumation ages and the U–Pb system yielding high-temperature cooling ages which help constrain the timing of apatite crystallization. This chapter focuses on integrating apatite fission track and U–Pb dating by the LA–ICP–MS method. The use of LA–ICP–MS to calculate U concentrations in fission track dating dramatically increases the speed of analysis and sample throughput compared to the conventional external detector method, as well as avoiding the need for neutron irradiation (*e.g.*, Hasebe *et al.* 2004). Other chemical composition data (*e.g.*, trace elements and the REE) can be acquired at the same time as U concentration data, and these data are very useful in detrital apatite provenance studies. Trace element compositional data are also highly useful for characterizing the thermal annealing kinetics of fission tracks in apatite and can be used in detailed time–temperature history modeling using programs such as HeFTy (Ketcham 2005).

Our analytical protocol for combined apatite fission track and U–Pb dating by LA–ICP–MS is outlined following summaries of both methods. Our approach is intentionally broad in scope, and should be applicable to any quadrupole or rapid-scanning magnetic-sector LA–ICP–MS system. Potential applications of combined apatite fission track and U–Pb dating and future trends in apatite provenance analysis are discussed at the end of this chapter.

OVERVIEW OF APATITE FISSION TRACK DATING

Fission track dating is a widely used technique for reconstructing the low-temperature thermal histories of upper crustal rocks. It has been used to study the tectonic and thermal histories of compressional and extensional margins, the stability of continental interiors, the thermal histories of sedimentary basins and their source regions, landscape evolution, and to constrain the timing of ore mineralization events. The method has been described and reviewed elsewhere (*e.g.*, Gleadow 1981, Gleadow *et al.* 1986a, Gleadow *et al.* 1986b, Green 1988, Gallagher *et al.* 1998, Donelick *et al.* 2005) and this chapter only presents a brief overview of the technique.

Fission track dating is based on the spontaneous fission decay of ^{238}U which produces linear defects in the lattice of U-bearing minerals (Fleischer *et al.* 1975, Price & Walker 1963). These linear defects are commonly referred to as fission tracks, and are enlarged using a standardized chemical etching process so they can be observed under an optical microscope (Price & Walker 1962). The technique is widely applied to apatite, zircon and titanite because they contain sufficient U (typically >10 ppm) to generate a statistically useful quantity of spontaneous fission tracks over geological time. By comparing the density of fission tracks with the U content of the mineral, an apparent fission track age can be calculated. A fission track age provides an estimate of the time that has elapsed since the mineral cooled through a specific temperature window (referred to as the partial annealing zone or PAZ). Apatite, zircon and titanite each have their own specific PAZ. The apatite PAZ is estimated at 60–110°C although this varies with apatite composition (Green *et al.* 1986, Carlson *et al.* 1999, Barbarand *et al*. 2003). At temperatures higher than the PAZ, there is sufficient energy to completely anneal (or remove) fission tracks via thermally activated diffusion of the relocated ionic species in the lattice. At temperatures lower than the PAZ, there is insufficient energy to cause significant repair of fission tracks. Fission tracks are partially annealed at temperatures within the PAZ.

To calculate the apparent fission track age of a mineral we need to i) estimate the amount of ^{238}U decay that is recorded in the mineral lattice and which is given by the spontaneous fission track density, and ii) estimate the amount of ^{238}U (the parent isotope). The spontaneous fission track density is calculated by counting etched fission tracks by optical microscopy. In most fission track dating studies the amount of ^{238}U is obtained after irradiation of the samples by thermally activated neutrons in a nuclear reactor. This approach, referred to as the external detector method (*e.g.*, Gleadow 1981) is described in the next section.

In addition to the fission track age which yields information on the timing of cooling through the PAZ, the apatite fission track method also yields information on the nature of the cooling path. This information is obtained from the distribution of confined fission track lengths in a sample (Gleadow *et al.* 1986a). Confined fission tracks are horizontal (or <10° from horizontal) tracks that lie in a c-axis prismatic section, such that both ends of the track are visible entirely within the polished and etched apatite crystal without altering the focal depth. Unannealed, spontaneous fission track lengths in natural apatite grains typically range between ~14.5

and 15.5 μm depending on its chemical composition (Gleadow *et al.* 1986a). For example, an apatite grain which exhibits a fission track population with mean track lengths in this range and a narrow variation in track length distribution (*e.g.*, <1.5 μm), would be interpreted to have cooled relatively rapidly from a temperature ≥ 110°C to a temperature ≤60°C at the time indicated by the apparent apatite fission track age. A shorter mean track length with a broad standard distribution indicates that the sample resided in the PAZ for a significant period of time since the formation of the oldest fission tracks (Gleadow *et al.* 1986b). The apatite fission track age and track length distribution can be combined to construct time–temperature paths by inverse and/or forward modeling of the fission track age and length data (*e.g.*, Gallagher 1995, Ketcham 2005).

Uranium concentrations by the external detector method

Uranium concentration measurements in fission track analysis have traditionally been undertaken using the external detector method (Gleadow 1981, Hurford & Green 1982, Gleadow *et al.* 1986b). The external detector method involves bombarding the apatite grain mount with thermal neutrons in a nuclear fission reactor to create induced fission tracks in the apatite sample. As the thermal-neutron capture cross-section of ^{235}U is significantly larger than that of ^{238}U, ^{234}U and ^{232}Th, thermal-neutron bombardment favors induced fission of ^{235}U with negligible fission of the other U and Th isotopes. The induced fission tracks are registered in both the apatite lattice (in which the spontaneous fission tracks have already been chemically etched) and an external detector, which is composed of low U (<1 ppm) muscovite and which is placed in intimate contact with the apatite grain mount. The induced fission track density in the external detector muscovite is therefore a function of the ^{235}U content (and hence the ^{238}U content) of the apatite assuming the natural $^{238}U/^{235}U$ ratio of 137.88 (Steiger & Jäger 1977).

Other parameters which influence the induced fission track density in the external detector muscovite include the neutron flux, the duration of irradiation and the neutron capture cross section of ^{235}U. The integrated thermal-neutron flux which infiltrates the apatite grain mount in the reactor is measured by determining the induced fission track densities of muscovite detectors which are placed in intimate contact with standard silicate glasses with known and homogeneously distributed U contents. The induced fission tracks registered in all the muscovite detectors are then chemically etched. Subsequently, the ^{238}U content of any specific portion of an apatite crystal can be determined by counting the induced fission tracks in the muscovite detector that was in contact with that region of the crystal.

Advantages and disadvantages of an LA–ICP–MS-based approach

LA–ICP–MS-based U concentration measurements in apatite fission track dating were first described in detail by Hasebe *et al*. (2004). Their approach used a 266 nm Nd:YAG laser attached to a quadrupole ICP–MS and involved rastering a 10 μm laser beam over a 50 × 50 μm square. To calculate a fission track age, the U content of the apatite needs to be measured on the same area that was counted for fission tracks. The total ablated area employed in the Hasebe *et al.* (2004) study was chosen as a 50 × 50 μm square as this most closely corresponded to the area that was counted for fission tracks. In-run variations in the ^{238}U signal intensity in both samples and standards (NIST 610 and 612 standard glasses) were normalized relative to the ^{44}Ca peak which was used to correct for variations in ablation volume. Calibration factors (relative signal intensity *versus* ^{238}U content) were then established for the standard glasses as their U concentrations and CaO contents are known independently. The ^{238}U content of the apatite unknowns can then be calculated using these calibration factors and assuming that Ca in apatite is stochiometric. Subsequent work by Hasebe *et al.* (2009) demonstrated that the chemical etching process required to reveal spontaneous fission tracks in apatite does not affect LA–ICP–MS-based U concentration measurements.

The chief advantage of U concentration measurements by LA–ICP–MS is that it dramatically increases the speed of analysis and sample throughput because it avoids the need for neutron irradiation. Neutron irradiation is time-consuming and logistically complicated as it involves the production, transport and handling of radioactive samples. Another advantage of an LA–ICP–MS approach using quadrupole or rapid-scanning magnetic-sector systems is that it enables multi-element analyses during a single ablation. In addition to facilitating U–Pb dating of apatite which is covered in detail later in this chapter, multi-element analyses in apatite are useful for both

characterizing the annealing behavior of fission tracks in apatite and for discriminating between different apatite populations in sedimentary or volcaniclastic rocks as described below.

The annealing behavior of fission tracks in apatite is not completely understood, but it is known to be highly temperature-dependent and moderately dependent upon crystallographic orientation. It is also dependent on parameters such as the chemical composition and crystal structure of the host apatite (*e.g.*, Green *et al*. 1985, Carlson *et al.* 1999, Barbarand *et al*. 2003). Fission track annealing models attempt to correlate fission track annealing kinetics with measurable parameters, commonly referred to as kinetic parameters, which take into account the variations in the chemical composition or etching characteristics of the host apatite (*e.g.*, Donelick 1993, Carlson *et al.* 1999, Barbarand *et al.* 2003). These kinetic parameters include Dpar, the fission track etch figure diameter parallel (or perpendicular, Dper) to the crystallographic c-axis, and the apatite chlorine content (measured by EPMA). Chlorine typically exerts the dominant control on apatite structure, but unfortunately it is difficult to analyze by ICP–MS due to its high first ionization potential. However at low chlorine contents the extent of cation substitution (in particular the REE) becomes more important and variations in REE concentration can be quantified by LA–ICP–MS analysis. An LA–ICP–MS approach also facilitates measurement of ^{232}Th and ^{147}Sm, which along with ^{235}U and ^{238}U are the principal alpha-emitting isotopes in apatite. Concentration measurements of these alpha-emitting isotopes in apatite will permit further understanding of the process of radiation-enhanced annealing described by Hendriks & Redfield (2005).

Trace element partition coefficients in igneous apatite are commonly very sensitive to changes in magmatic conditions and can exhibit large variations in concentrations. The trace element composition of igneous apatite can therefore be a useful diagnostic tool in igneous petrogenesis studies (Sha & Chappell 1999; Jennings *et al.* 2011). This petrogenetic information can be inverted to yield useful provenance information – for example volcanogenic apatite trace element concentrations (Mg, Cl, Mn, Fe, Y, and Ce) have been applied to tephra correlation problems in the eastern U.S. and between North America and Europe (Sell & Samson 2011). Additionally apatite REE geochemistry has been demonstrated to have significant potential in geochemical exploration (Belousova *et al.* 2002) and sandstone provenance studies (Dill 1994; Morton & Yaxley 2007). The REE and trace element suites described above can be analyzed simultaneously with U and Pb isotopes by LA–ICP–MS.

However there are potential challenges associated with an LA–ICP–MS-based approach to U concentration measurements. The main difficulty is ensuring that the U distribution with the portion of sample that generates fission tracks on the polished apatite surface is quantified spatially, both horizontally (*i.e.*, along the surface of the grain mount) and vertically. One of the major strengths of the external detector approach is that data are collected from identical areas on individual grains and their mirror images in the muscovite detector, and therefore within-grain heterogeneity in U concentration can be accommodated by this technique. The distribution of induced tracks in the external detector can therefore be considered as a reliable proxy map for the U distribution in its mirror image apatite grain. This induced track "map" also records depth-integrated variations in U concentration, as induced fission (similar to spontaneous fission) generates tracks in the detector that are produced by U up to half a fission track length below the apatite grain surface.

It is therefore very important that U concentrations are collected from the same area that was employed for apatite fission track counting. As it is impractical with most laser ablation systems to change the raster area dimensions from grain to grain (particularly during automated data acquisition runs), multiple raster or spot analyses are appropriate when the counted area is large. Down-hole variations in U concentration also need to be taken into account. The "effective" U concentration of a spot analysis needs to be depth integrated so that U concentration data close to the grain surface are weighted more heavily than U concentrations at depth. The analysis pit needs to extend to a distance of 10 μm (broadly half a fission track length) below the apatite grain surface and it is therefore also important that the depth of the ablated spot can be calculated accurately.

Another potential challenge in LA–ICP–MS-based measurements of U concentrations in apatite arises if the internal standard (typically ^{43}Ca) is non-stochiometric. Divalent minor cations such as Mn^{2+}, Sr^{2+}, Ba^{2+} and Fe^{2+} exhibit simple substitution with Ca^{2+} and can be quantified by multi-elemental LA–ICP–MS analyses. However trivalent cations such

as the REE are envisaged to undergo more complex charge-coupled substitutions such as $REE^{3+} + Si^{4+} \rightleftharpoons Ca^{2+} + P^{5+}$ and $REE^{3+} + Na^{+} \rightleftharpoons 2Ca^{2+}$ (Rønsbo 1989), and the extent of Ca^{2+} substitution may therefore be harder to quantify accurately.

U–PB APATITE DATING BY LA–ICP–MS

Low U, Th and radiogenic Pb concentrations, elevated common Pb to radiogenic Pb ratios, and limited availability of suitable U–Pb apatite standards (to correct for U–Pb elemental fractionation) remain significant challenges in dating apatite by LA–ICP–MS. The problems of correcting for common Pb and U–Pb elemental fractionation are discussed in more detail later in this section.

Early studies focused on ^{207}Pb–^{206}Pb dating of Paleoproterozoic samples by multi-collector LA–ICP–MS (Willigers *et al.* 2002). Although ^{207}Pb–^{206}Pb dating removes the need for a matrix-matched standard, it eliminates the ability to evaluate concordance and is of limited application to dating Phanerozoic apatite grains due to the difficulty in obtaining precise ^{207}Pb–^{206}Pb ratios from young samples. Storey *et al.* (2007) dated Paleoproterozoic apatite mineralization in the Norrbotten iron ore province in Sweden by quadrupole ICP–MS. Common Pb was sufficiently low as to not necessitate a common Pb correction, while U/Pb ratios in apatite were corrected using the 91500 zircon standard. The U–Pb apatite ages were moderately reversely discordant due to possible elemental fractionation of Pb and U isotopes relative to the external standard during laser ablation. Carrapa et al. (2009) dated detrital apatite from Cenozoic basins of the central Andean Puna plateau by multi-collector ICP–MS. U/Pb laser-induced fractionation was constrained by analysis of Bear Lake Road titanite (1050 ± 1 Ma), a Sri Lanka zircon crystal (563.5 ± 3.2 Ma) and NIST SRM 610 trace element glass. Common Pb correction employed the measured ^{204}Pb assuming an initial Pb composition from Stacey & Kramers (1975).

Chew *et al.* (2011) determined U–Pb and Th–Pb ages for seven well known apatite occurrences (Durango, Emerald Lake, Kovdor, Mineville, Mudtank, Otter Lake and Slyudyanka) by LA–ICP–MS. Analytical procedures involved rastering a 10 μm spot over a 40 × 40 μm square using a 193 nm ArF excimer laser coupled to a Thermo ElementXR single-collector ICP–MS. These raster conditions minimized laser-induced inter-element fractionation, which was corrected for using the back-calculated intercept of the time-resolved signal. A Tl–U–Bi–Np tracer solution was aspirated with the sample into the plasma to correct for instrument mass bias. External standards (Plešovice and 91500 zircon, NIST SRM 610 and 612 silicate glasses and STDP5 phosphate glass) and Kovdor apatite were analyzed to monitor U–Pb, Th–Pb and Pb–Pb ratios. Common Pb correction employed the ^{207}Pb method, and also a ^{208}Pb correction method for samples with low Th/U. The ^{207}Pb and ^{208}Pb corrections employed either the initial Pb isotopic composition where known or the Stacey and Kramers model. No ^{204}Pb correction was undertaken because of ^{204}Pb interference by ^{204}Hg in the argon gas supply. Age calculations used a weighted average of the common Pb-corrected ages and Tera-Wasserburg concordia intercept age (both un-anchored and anchored through common Pb). The samples yielded ages consistent with independent estimates of the U–Pb apatite age, with weighted mean age uncertainties as low as 1–2% for U- and/or Th-rich Paleozoic–Neoproterozoic samples.

Thomson *et al*. (2012) presented apatite U–Pb data acquired using a Nu Plasma multi-collector ICP–MS coupled to a short pulse ArF excimer laser. Two new matrix-matched reference apatite grains were presented to correct for elemental fractionation: a gem quality 485 Ma apatite from Madagascar which was independently characterized by ID–TIMS analysis, and 523.5 Ma apatite from the McClure Mountain syenite (Schoene & Bowring 2006). Common Pb was corrected using the measured ^{204}Pb corrected for ^{204}Hg interference and a five step iterative process using the Stacey & Kramers (1975) terrestrial Pb evolution model. The study of Thomson *et al*. (2012) regularly achieved accurate ages on independently characterized apatite grains with a precision of <2% (2σ) by pooling as few as five 30 μm spot analyses. Young and /or low U apatite necessitated a larger spot size (65μm) to yield a ^{207}Pb signal large enough to be measured on a Faraday collector.

Common Pb correction methods

Arguably, the major limitation on the accuracy and precision of apatite age determinations is the need to use common Pb correction. Common Pb correction methods typical involve either i) concordia or isochron plots on a suite of cogenetic apatite grains with a large spread in common Pb to radiogenic Pb ratio or ii) Pb correction based on an appropriate choice of initial Pb isotopic composition.

i) Several Pb correction methods do not require an estimate of the initial Pb isotopic composition. They typically require several analyses of a suite of cogenetic apatite grains with a significant spread in common Pb/radiogenic Pb ratios to define a well constrained linear array on a concordia diagram or isochron. The total-Pb/U isochron, a three-dimensional $^{238}U/^{206}Pb$ *vs* $^{207}Pb/^{206}Pb$ *vs* $^{204}Pb/^{206}Pb$ plot (Ludwig 1998), yields the smallest error of any possible U/Pb or Pb/Pb isochron as all relevant isotope ratios are employed. Discordance and variation in the initial Pb composition of the suite of analyzed grains on a Total-Pb/U isochron can be assessed by the MSWD of the regression. Other isochrons, such as the $^{238}U/^{204}Pb$ *vs* $^{206}Pb/^{204}Pb$, $^{235}U/^{204}Pb$ *vs* $^{207}Pb/^{204}Pb$, $^{232}Th/^{204}Pb$ *vs* $^{208}Pb/^{204}Pb$ and $^{207}Pb/^{204}Pb$ *vs* $^{206}Pb/^{204}Pb$ plots assume the U–Pb* data (where Pb* = the radiogenic Pb component) are concordant in order to calculate isochron dates. This assumption of concordance can be difficult to assess but can be evaluated to some extent by the MSWD of the regression. Another approach (*e.g.*, Simonetti *et al.* 2006) involves projecting an intercept through the uncorrected data on a Tera–Wasserburg concordia to determine the common Pb component (y-intercept) on the $^{207}Pb/^{206}Pb$ axis. The $^{238}U/^{206}Pb$ age can then be calculated as a lower intercept age on the $^{238}U/^{206}Pb$ axis (x-intercept) or as a weighted average of ^{207}Pb-corrected ages (see below) using the concordia $^{207}Pb/^{206}Pb$ intercept as an estimate of the initial Pb isotopic composition. This approach also assumes that the U–Pb* data are concordant and equivalent.

ii) The second set of common Pb correction methods involves correcting individual analyses for initial Pb. Three methods are commonly employed in the literature, the ^{204}Pb-, ^{207}Pb- and ^{208}Pb-correction methods (*e.g.*, Williams 1998). Estimates of the initial Pb isotopic compositions are typically derived from Pb evolution models (*e.g.*, Stacey & Kramers 1975). Alternatively it can be estimated by analyzing a low U co-magmatic phase (*e.g.*, K-feldspar or plagioclase) which exhibits negligible in-growth of radiogenic Pb, but this approach is typically not feasible for the analysis of detrital minerals. The ^{204}Pb correction method is potentially the most powerful as it does not assume U/Pb* concordance. It does require accurate measurement of ^{204}Pb and is sensitive to the low $^{206}Pb/^{204}Pb$ ratios encountered in Phanerozoic samples (*e.g.*, Cocherie *et al.* 2009). It is thus ideally suited to U–Pb dating by high precision ID–TIMS or MC–ICP–MS analysis (*e.g.*, Gehrels *et al.* 2008, Thomson *et al.* 2012), as low ^{204}Pb concentrations can be measured accurately. The ability to identify concordance in the ^{204}Pb-corrected data is also advantageous although concordance can be obscured by an inappropriate choice of initial Pb (*e.g.*, by using Pb evolution models).

Both the ^{207}Pb- and ^{208}Pb-correction methods assume initial concordance in $^{238}U/^{206}Pb$–$^{207}Pb/^{206}Pb$ and $^{238}U/^{206}Pb$–$^{208}Pb/^{232}Th$ space, respectively. The ^{207}Pb-correction method is commonly used in U–Pb ion microprobe studies (Gibson & Ireland 1996), and only requires precisely measured $^{238}U/^{206}Pb$ and $^{207}Pb/^{206}Pb$ ratios and an appropriate choice of common Pb. The ^{208}Pb-correction method is less commonly applied. It requires the measurement of $^{208}Pb/^{206}Pb$ and $^{232}Th/^{238}U$ and an appropriate choice of initial $^{208}Pb/^{206}Pb$, and works well for samples with low Th/U (*e.g.*, <0.5) (Cocherie 2009, Williams 1998).

As the goal of this chapter is to integrate apatite fission track and U–Pb dating by LA–ICP–MS (with particular reference to apatite provenance studies), it is imperative that the adopted common Pb correction method is compatible with this goal. Isochron-based approaches require several analyses with a significant spread in common Pb to radiogenic Pb ratios to define a well constrained linear array on a concordia diagram or isochron. This is not usually possible on individual detrital apatite grains, and so the ^{204}Pb-, ^{207}Pb- and ^{208}Pb-correction methods are more appropriate. However, U concentration measurements by ICP–MS require large peak jumps as the internal standard used for normalizing the ^{238}U signal is typically ^{43}Ca. This ideally requires a quadrupole or rapid-scanning single-collector magnetic-sector LA–ICP–MS system, as fast peak hopping through a number of elements is not usually practical on most multi-collector ICP–MS systems due to the excessive time it takes for the magnet to settle. However on single collector instruments it often requires a prohibitively long dwell time on the low intensity ^{204}Pb peak to measure it accurately, particularly if there is ^{204}Pb interference caused by ^{204}Hg in the argon gas supply. This means that the ^{207}Pb- and ^{208}Pb-correction methods are usually preferred to the ^{204}Pb-correction method. However these Pb-correction methods need estimates of the initial Pb isotopic composition. For detrital apatite samples these can be derived from Pb evolution models (*e.g.*, Stacey & Kramers 1975) using a starting estimate for the age of the apatite and adopting an iterative approach (Chew *et al.* 2011, Thomson *et al.* 2012).

U–Pb elemental fractionation

Elemental fractionation is an important consideration in U–Pb dating of accessory minerals by LA–ICP–MS. Elemental fractionation takes place at the site of ablation (laser-induced fractionation) while the mass discrimination (bias) of the ICP–MS instrument also needs to be taken into account. Several techniques have been used both to minimize this fractionation and to correct for it, primarily in U–Pb dating studies of zircon, and the reader is referred to Košler & Sylvester (2003) for a detailed account of these techniques.

The most common approach is to use a standard for external calibration of down-hole fractionation of Pb and U. A matrix-matched standard is typically required because LA–ICP–MS dating of different accessory minerals (*e.g.*, apatite, titanite and zircon) typically shows different time-resolved Pb/U signals during ablation (Gregory *et al.* 2007). Analysis of the matrix-matched standard produces an empirical correction factor that can be applied to the unknown sample (*e.g.*, Jackson *et al.* 1996). The Pb/U ratios of the standard are measured before and after analysis of the unknown, and a correction factor (ratio) between the true standard age and the measured age of the standard is calculated. The true age (Pb/U ratio) of the unknown can then be derived from the measured sample ratios using this correction factor. These data need also be corrected for instrument drift (change in sensitivity with time) prior to correction for elemental fractionation. This method assumes instrument parameters remain constant between analysis of the standard and the unknown, and there are no significant matrix effects on the measured Pb/U and Pb isotopic ratios between the standard and the sample. This method requires a well characterised U–Pb mineral standard.

A second approach to correct for Pb/U elemental fractionation is that of Košler *et al.* (2002), which is based on the premise of Sylvester & Ghaderi (1997) that laser-induced, volatile/ refractory element fractionation is a linear function of time, and therefore it can be corrected by extrapolating the measured ratios back to the start of ablation. Pb/U ratios at the start of laser ablation therefore are biased only by the mass discrimination (bias) of the ICP–MS instrument which is corrected by aspirating a tracer solution (*e.g.*, Tl–U–Bi–Np) with the sample into the plasma. The fractionation-corrected Pb/U isotopic ratios are calculated as zero ablation time intercepts of least squares linear regression lines fitted to the time-resolved isotopic ratio data. This correction eliminates potential matrix differences between external standards and unknown samples because the intercept is calculated from the data for each individual sample. This method has been applied to U–Pb LA–ICP–MS dating of zircon (Košler *et al.* 2002), monazite (Košler *et al*. 2001), perovskite (Cox &Wilton 2006) and apatite (Chew *et al.* 2011). Although simultaneous aspiration of the tracer solution does result in decreased sensitivity and increased oxide production, this approach is well suited to target minerals for which no matrix-matched standard exists.

The analytical uncertainty due to the elemental fractionation corrections increases with the size of the correction and it is therefore important to minimize fractionation. Various laser parameters can be used to suppress fractionation, and it may also be reduced by scanning the stage beneath the stationary laser beam. This produces a linear traverse or raster in the sample (Košler *et al.* 2002), and the effect is similar to ablating a large shallow laser pit, which produces only limited Pb/U fractionation (Eggins *et al.* 1998, Mank & Mason 1999).

SUGGESTED ANALYTICAL PROTOCOLS

Our analytical protocol for combined apatite fission track and U–Pb dating by LA–ICP–MS is intentionally broad in scope, and should be applicable to any quadrupole or rapid-scanning magnetic-sector LA–ICP–MS system. Combined U–Pb dating and U concentration measurements for fission track dating require measurement of the ^{43}Ca peak as an internal standard and ideally should also include the suite of commonly occurring minor cations in apatite (*e.g.*, Mn, Fe, Mg, Fe, Sr, Ba, Y and REE) to ensure that the cation substitution for Ca is accurately quantified. These minor cations may also provide additional provenance information. However these large peak jumps are impractical on multi-collector ICP–MS systems. Even rapid-scanning magnetic-sector ICP–MS systems such as the Thermo Element or Nu AttoM (which combine fast-scanning magnets with electric peak jumps of between 30–40% of the relative mass range) can acquire typically only ~10% of the data scans compared to a quadrupole-based ICP–MS system for a given analysis time.

Sample preparation and imaging of fission track samples

A variety of methods have been developed for apatite fission track sample preparation although it

is beyond the scope of this chapter to discuss and compare all of these methods in detail. The reader is referred to Donelick *et al.* (2005) for a comprehensive review and for the sample preparation methods used in this study. The fission track data acquired for the case studies later in this chapter (R.A.D.) were viewed and counted or measured at 1562.5x dry magnification using unpolarized transmitted light and a Nikon Optiphot2 microscope. All fission track age and length grains were selected to sample the range of observable characteristics (*e.g.*, grain size, degree of roundness, color and variations in Dpar). Unlike the external detector method in fission track dating, LA–ICP–MS is a destructive technique. It is therefore important to store high quality 3-D images of the tracks in the apatite in both reflected and transmitted light so that the analyzed grains can be archived for potential reinvestigation in the future. Many of the new fission track dating systems which are designed for automated counting (*e.g.*, Gleadow *et al.* 2009) are also well suited for this purpose as they are equipped with high resolution digital cameras and the ability to control the Z-focus of the microscope stage with sub-micron resolution and reproducibility.

Matrix-matched standards

There are presently only a few well characterized U–Th–Pb apatite standards. Seven potential apatite standards (Durango, Emerald Lake, Kovdor, Mineville, Mudtank, Otter Lake and Slyudyanka) were investigated in the study of Chew *et al*. (2011). Of these, Kovdor (387±8.2 Ma; U = 56 ppm, Th = 3540 ppm, Pb = 65 ppm), Emerald Lake (92.5±3.3 Ma; U = 47 ppm, Th = 122 ppm, Pb = 3.2 ppm) and Slyudyanka apatite (448±7.3 Ma; U = 94 ppm, Th = 202 ppm, Pb = 18 ppm) were suggested to have most potential, with the Durango apatite (31.44 Ma, McDowell *et al.* 2005) making a suitable secondary standard. The Kovdor carbonatite apatite was recommended as the best potential U–Pb and Th–Pb apatite standard for LA–ICP–MS analyses by Chew *et al.* (2011) as the crystallization age and initial Pb isotopic composition are known from high precision TIMS analyses (Amelin & Zaitsev 2002) and it yielded high U, Th and Pb concentrations. However apatite from the Kovdor carbonatite is very variable in terms of its U and Th concentrations and the lower U and Th concentrations (typically 1–10 ppm U, 60–150 ppm Th) documented by Amelin and Zaitsev (2002) are probably more typical.

In this study, McClure Mountain syenite apatite, one of the two apatite standards used by Thomson *et al.* (2012), is used as the primary standard. It is suitable as a standard as it has moderate but reasonably consistent U and Th contents (~23 ppm and 71 ppm; this study), its thermal history is well known (it is the rock from which the $^{40}Ar/^{39}Ar$ hornblende standard MMhb is derived) and importantly the crystallization age (weighted mean $^{207}Pb/^{235}U$ date of 523.51 ± 2.09 Ma) and initial Pb isotopic composition ($^{206}Pb/^{204}Pb$ = 17.54 ±0.24; $^{207}Pb/^{204}Pb$ = 15.47 ±0.04) are known from high precision TIMS analyses (Schoene & Bowring 2006). Durango apatite and Duluth Complex apatite (U–Pb zircon age of 1099.1 ±0.2 Ma, Schmitz *et al.* 2003) were used as secondary standards. Tertiary standards which were analyzed at the start and end of analytical sessions include Mount Dromedary apatite ($^{40}Ar/^{39}Ar$ biotite age of 99.17 ± 0.48 Ma, Renne *et al.* 1998) and Fish Canyon Tuff apatite (astronomically calibrated age of 28.201 ± 0.012 Ma; Kuiper *et al.* 2008).

Laser and ICP–MS parameters

The data presented in the integrated apatite fission track and U–Pb dating case study at the end of this chapter were acquired using a Resonetics M-50 193 nm ArF Eximer laser-ablation system coupled to an Agilent 7700x quadrupole ICP–MS at the Donelick Properties laboratory in Viola, Idaho, U.S.A. Laser ablation was performed using a 26 µm spot and a 7 Hz laser repetition rate with the laser set in constant energy mode. Spot ablations were chosen over rastering as the ablation depth can be well constrained in spot analyses and this information is required for depth-integrated U concentration measurements. The enhanced laser-induced U–Pb fractionation produced by spot analyses is accounted for during data reduction (see below). Data collection by the ICP–MS was triggered upon arrival at a spot and comprised a 6 s delay and 34 s ablation time followed by a 20 s delay before the laser was positioned at the next spot and the sequence was repeated. Ablated material was transported to the plasma using ultra-high purity He and N_2 both of which were passed through an inline Hg trap. High purity Ar was employed as the plasma gas.

A total of 41 isotopes were analyzed in a typical apatite sample (Table 12-1). Of these, ^{43}Ca was used as an internal standard to correct for variations in ablation volume while ^{202}Hg was used to monitor interference on the ^{204}Pb peak by ^{204}Hg

in the argon gas supply. Common trace elements in apatite (including Na, Mg, Si, Mn, Fe, Sr, Y and Ba) and the REE were analysed along with the six isotopes (^{204,206,207,208}Pb, ^{232}Th and ^{238}U) commonly employed in U–Th–Pb geochronology. In addition, anions with high first ionization potentials (S: 10.36 eV, Cl: 12.97 eV, and Br: 11.81 eV) which are characterized by relatively low sensitivities and also polyatomic isobaric interferences (in particular S and Cl) were measured as part of a preliminary study investigating the potential of LA–ICP–MS analyses of these anions in apatite. The dwell time on each element was typically 1 ms with notable exceptions including ^{43}Ca, ^{202}Hg, ^{204,206,207,208}Pb, ^{232}Th and ^{238}U where significantly longer dwell times were employed (Table 12-1). Element concentrations can be obtained through calibration of the relative element sensitivities using NIST-610 glass as the external standard, and normalization of each analysis to the ^{43}Ca peak as an internal standard to determine the ablation yield. The reference data for the NIST 610 calibration standard glass are given by Norman *et al.* (1996). Alternatively, as in this study, a well characterized crystal of Durango apatite can be used as an external standard.

DATA REDUCTION SCHEMES FOR U–PB DATING AND U CONCENTRATION MEASUREMENTS

Two approaches are outlined here for data reduction in apatite U–Pb dating and U concentration measurements by ICP–MS. The two data reduction packages were derived independently but are similar from a theoretical viewpoint. The first approach (R.A.D.) uses custom-written software (FTUPbICP) for ICP–MS data processing and is described in detail in the Appendix while the second approach (D.M.C.) uses the freeware IOLITE data reduction package of Paton *et al.* (2010, 2011) combined with the VizualAge data reduction scheme of Petrus & Kamber (in press). Both approaches involve processing an entire analytical session of data which is not only more efficient but also greatly improves the consistency and reliability of data reduction.

The first step in both approaches is to define the baseline values for each isotope during the course of the analytical session. This is performed automatically by FTUPbICP by detecting synchronous global minima in the ^{232}Th and ^{238}U signals; IOLITE offers the user a choice of automatic or user-defined time intervals for the baseline correction. In both cases session-wide baseline-corrected values for each isotope are then calculated.

Correcting for common Pb and laser-induced fractionation

Both approaches use a similar approach to quantifying laser-induced elemental (*i.e.*, U–Th–Pb) fractionation. Both methods involve characterizing the time-resolved fractionation response of individual standard analyses and then fitting an appropriate session-wide "model" U–Th–Pb fractionation curve to the time-resolved standard data. This fractionation model is then applied to the

TABLE 12-1. ISOTOPES ANALYZED ON THE AGILENT 7700X SYSTEM (R.A.D.)

Isotope	Acquisition Time (ms)	Isotope	Acquisition Time (ms)	Isotope	Acquisition Time (ms)	Isotope	Acquisition Time (ms)
^{23}Na	1	^{56}Fe	1	^{146}Nd	1	^{178}Hf	1
^{24}Mg	1	^{75}As	1	^{147}Sm	1	^{202}Hg	12.6
^{27}Al	1	^{79}Br	3	^{151}Eu	1	^{204}Pb	150
^{29}Si	1	^{88}Sr	1	^{157}Gd	1	^{206}Pb	150
^{31}P	1	^{89}Y	1	^{159}Tb	1	^{207}Pb	150
^{32}S	1	^{91}Zr	1	^{163}Dy	1	^{208}Pb	150
^{35}Cl	3	^{127}I	3	^{165}Ho	1	^{232}Th	12.5
^{39}K	1	^{138}Ba	1	^{166}Er	1	^{238}U	12.5
^{43}Ca	3	^{139}La	1	^{169}Tm	1		
^{47}Ti	1	^{140}Ce	1	^{172}Yb	1		
^{55}Mn	1	^{141}Pr	1	^{175}Lu	1		

unknown samples. The advantage of this approach is that it has the versatility to treat data from any laboratory, regardless of the expression of the downhole fractionation. The standard data (typically McClure Mountain syenite apatite) are corrected for common Pb using the ^{207}Pb-correction method (FTUPbICP).

Results of the age standards

Age standard data are presented in Figure 12-1. For the Agilent 7700x quadrupole ICP–MS set-up and using the FTUPbICP software for ICP–MS data processing, 19 analyses of McClure Mountain apatite (not used in the standard calibration) yielded a weighted average ^{207}Pb-corrected ^{206}Pb/^{238}U age of 522 ±14 Ma (2σ; MSWD = 0.97, Fig. 12-1a). The 2σ precision on an individual analysis is about ±60 Ma (12%). 45 analyses of Durango apatite yield a weighted average ^{207}Pb-corrected ^{206}Pb/^{238}U age of 33 ±2.4 Ma (2σ; MSWD = 1.3; Fig. 12-1b), with a 2σ precision on an individual analysis of about ±15 Ma (50%). For comparison, high precision multi-collector LA–ICP–MS standard data are presented in Figures 12-1c and 12-1d. These data were reduced using the IOLITE package and are similar in precision to the study of Thomson *et al.* (2012). They were acquired using a NEPTUNE MC–ICP–MS coupled with a New Wave 193 nm excimer laser at the National Centre for Isotope Geochemistry (NCIG) at UCD, Dublin. Ion counters were used to measure ^{202}Hg, ^{204}Pb+Hg, ^{206}Pb, ^{207}Pb, ^{208}Pb and ^{238}U. ^{232}Th was measured on

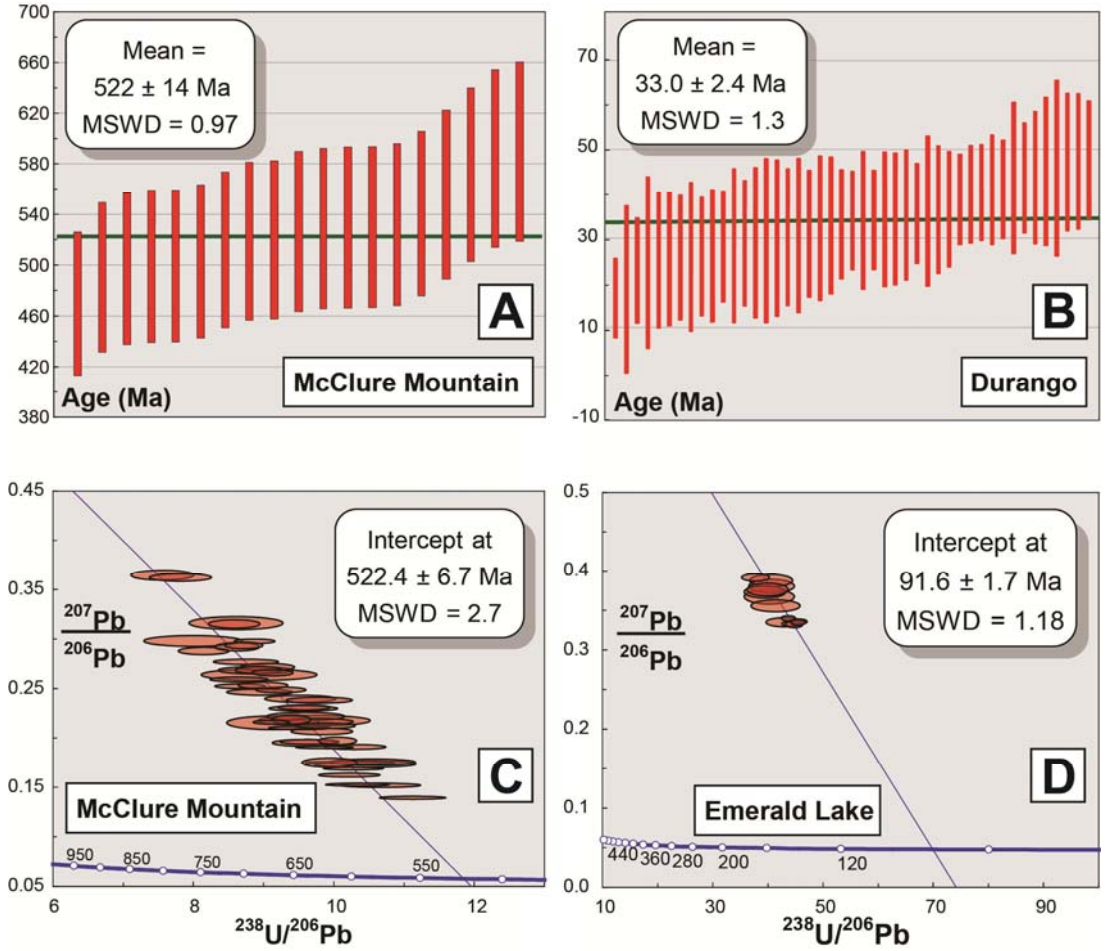

FIGURE 12-1. U–Pb apatite standard data. Data in **(a, b)** were acquired using an Agilent 7700x quadrupole ICP–MS coupled to a Resonetics 193 nm ArF Eximer laser-ablation system. The spot size was 26 µm and the data are presented as weighted mean ^{207}Pb-corrected ^{206}Pb/^{238}U ages. Standard data in **(c,d)** were acquired using a Neptune MC- ICP–MS coupled to a New Wave193 nm ArF Eximer laser-ablation system. The spot size was 35 µm and the calculated ages are Tera-Wasserburg concordia lower-intercept ages anchored through common Pb.

a Faraday detector and the typical spot size was 35 μm. Forty-seven analyses of McClure Mountain apatite yield an anchored lower intercept Tera-Wasserburg concordia age of 522.4 ± 6.7 Ma (2σ; MSWD = 2.7, Fig. 12-1c). The 2σ precision on an individual analysis is about ± 20 Ma (4%). 12 analyses of Emerald Lake apatite yield an anchored lower intercept Tera-Wasserburg concordia age of 91.6 ± 1.7 Ma (2σ; MSWD = 1.18; Fig. 12-1d), with a 2σ precision on an individual analysis of about ±4.5 Ma (5%).

POTENTIAL APPLICATIONS IN PROVENANCE STUDIES

Apatite has many potential applications in sedimentary provenance studies, and offers some advantages compared to zircon. Detrital zircon studies (particularly U–Pb age dating) have been widely employed to investigate stratigraphic correlations, the identification of sediment sources and the transport and depositional histories of clastic rocks. Zircon is chemically and mechanically very stable, and it yields very reliable U–Pb age information due to its typically high U concentrations and minimal incorporation of common Pb during crystallization. U–Pb age information can also be supplemented by low temperature thermochronometric techniques on the same zircon crystals (such as fission track or (U–Th)/He dating) to constrain the exhumation history of the grains. Additionally most zircon crystals contain 0.5–2.0wt % HfO_2 but very low Lu/Hf ratios, typically ~0.002 (Kinny 2003). Zircon effectively therefore preserves the initial $^{176}Hf/^{177}Hf$ ratio, providing a record of the Hf isotopic composition of the source environment at the time of crystallization. The Hf isotopic composition of zircon can be utilized as a geochemical tracer of a host rock's origin in an analogous manner to the Sm–Nd isotopic system.

However, the chemical and mechanical robustness of zircon is also a disadvantage in sedimentary provenance studies as it can be recycled through one or more intermediary sediments or sedimentary rocks (Dickinson & Gehrels 2009), thus introducing a natural bias which is often difficult to quantify without resorting to additional analytical methods. For example U–Pb age-dating of zircon from modern day sediment samples in the Indus and Ganges rivers suggests only 2.5% of the Ganges zircon and 18% of the Indus zircon are unequivocally derived from the Himalaya or Tibetan Plateau (Campbell *et al*. 2005). However the very young ages obtained from (U–Th)/He dating of the same zircon grains suggests that over 95% of the zircon is derived from the Himalaya or Tibetan Plateau, suggesting the majority of Indus and Ganges zircon grains were originally recycled from older sedimentary rocks. Additionally, zircon does not occur in every crustal rock; it is most common in igneous rocks of intermediate to Si-saturated composition and less common in less saturated rocks (Hoskin & Schaltegger 2003). It is also difficult to link zircon to its parent rock type based on its trace element chemistry (*e.g.*, variations in Hf, Y, REE, Th and U contents). For example, the REE patterns for continental crustal zircon populations from rock-types such as igneous charnockite, gabbro, diorite, dacite, granite and aplite are all generally similar (*e.g.*, Hoskin & Schaltegger 2003). However Schoene *et al.* (2010) have shown that zircon exhibits a wide variation in trace element concentrations between different samples and rock compositions and can record petrogenetic processes such as fractional crystallization, assimilation and/or magma mixing.

Advantages of apatite over zircon in provenance analysis

Apatite is more likely to represent first-cycle detritus than zircon and it can yield reliable U–Pb age information assuming challenges such as low U, Th and radiogenic Pb concentrations and elevated common Pb / radiogenic Pb ratios can be overcome. Like zircon, apatite U–Pb age information can also be supplemented by low temperature thermochronometric techniques on the same crystals (such as combined apatite U–Pb and fission track dating which is the main focus of this chapter) to constrain the exhumation history of the grains. The Sm–Nd isotope system can also be applied to apatite (*e.g.*, Foster & Vance 2006) in a manner similar to the Lu–Hf isotope system in zircon, with the Nd isotopic composition providing a record of the Nd isotopic composition of the source environment at the time of apatite crystallization. The trace element partition coefficients in igneous apatite are typically more sensitive to changes in magmatic conditions than in zircon and the trace element chemistry of detrital apatite can provide an effective link to the parent igneous rock type in provenance studies.

EXAMPLE DATASET

The applications of combined apatite U–Pb, fission track, and trace element datasets fall broadly into two categories depending on the extent of post-depositional annealing that the detrital apatite

samples have experienced. If the samples remained below the temperature of the apatite PAZ (60–110°C) following deposition, then the apatite U–Pb and fission track data yield constraints on the high temperature and low temperature thermal history of the source region respectively, with the apatite trace element composition data yielding information on the nature of the parent igneous rock type. If the samples were heated above the temperature of the apatite PAZ following deposition, then the fission track data yield constraints on the thermal history of the host sedimentary rock. In addition to the U–Pb and trace element data providing information on the high temperature thermal history and nature of the igneous source, the U–Pb data may suggest the presence of discrete detrital apatite populations. The trace element compositional data may also prove useful for characterizing the annealing behavior of these discrete apatite populations.

Apatite fission track age and length measurements (Tables 12-2a, 2b) and U–Pb age determinations were performed on two samples from east-central Utah.

TABLE 12-2A. APATITE FISSION-TRACK LENGTH DATA.

Sample	Attem-pted spots	Accept-able spots	Ns (tracks)	P (x 10^{-3})	σ_P (x 10^{-3})	Mean Dpar (µm)	Mean Dper (µm)	ζ	σ_ζ	χ^2	Q(χ^2)	Pooled Age (Ma) (- + 95% confidence interval)
Standard: Primary Zeta Calibration for 31.44 Ma DR												
Durango (DR)	440	430	4275	1.8912	0.0012	1.86	0.38	13.9423	0.2171	521.53	0.001	31.44 -1.34 +1.40
This Study												
171-01	310	250	2712	0.8580	0.0207	2.23	0.58	13.9423	0.2171	1447.72	0.000	43.92 -3.62 +4.09
171-03	110	92	597	0.2661	0.0116	2.04	0.43	13.9423	0.2171	86.07	0.627	31.20 -3.62 +4.09

(analyst R.A.D.)

TABLE 12-2B. APATITE FISSION-TRACK LENGTH DATA

Sample	Mean (µm)	Standard Deviation (µm)	Skewness	Tracks	Mean Dpar (µm)	Mean Dper (µm)
Standards: Unannealed Induced Fission Tracks						
Durango DR H0	16.21 ± 0.07	0.75	0.15	110	1.83	0.43
Durango DR 458-14	16.46 ± 0.06	0.86	-0.14	153	not measured	not measured
Durango DR DRA5	16.37 ± 0.06	0.78	-0.29	200	1.91	0.52
Durango DR DRA5b	16.43 ± 0.06	0.82	-0.10	210	1.84	0.42
Fish Canyon Tuff IF H0	16.39 ± 0.09	0.87	-0.10	102	2.43	0.83
Tioga Bed B TI H0	16.45 ± 0.08	0.80	-0.22	110	2.45	0.80
Standards: Natural Fission Tracks						
Durango DR 01d	14.56 ± 0.09	0.92	-0.21	100	1.91	0.49
Durango DR 458-05	14.41 ± 0.09	1.02	-0.15	129	1.93	0.45
Durango DR 458-10	14.49 ± 0.09	1.04	-0.62	147	not measured	not measured
Durango DR 458-14	14.35 ± 0.08	0.99	-0.49	142	not measured	not measured
Durango DR nat1	14.55 ± 0.12	1.15	0.43	94	1.84	0.35
Durango DR nat2	14.44 ± 0.10	0.93	-0.19	80	1.80	0.36
Duluth Complex FC 01d	15.12 ± 0.10	1.03	-0.60	100	2.38	0.69
Duluth Complex FC nat1	14.99 ± 0.08	0.91	-0.29	135	2.38	0.61
Duluth Complex FC nat2	15.14 ± 0.08	0.97	0.09	133	2.43	0.65
Mount Dromedary MD 01c	13.88 ± 0.11	1.40	-1.63	150	1.72	0.38
Tioga Bed B TI 2001b	13.71 ± 0.15	2.15	-1.56	203	2.36	0.74
This Study: Natural Fission Tracks						
171-01	12.37 ± 0.07	2.02	-0.23	732	2.43	0.65
171-03	14.64 ± 0.08	1.18	-0.63	210	2.08	0.44

(analyst R.A.D.)

Sample 171-01 (N38°40.772' W109°25.210'). This sandstone sample, including what appears to be a <1 cm ash layer, was collected from the Lower–Middle Triassic Moenkopi Formation (Hunt 1958) at the northern end of Castle Valley near Moab, Utah. The sample locality occurs near the Colorado River base level in a wide canyon nearly 0.75 km deep.

Sample 171-03 (N38°34.210' W109°17.698'). This alkaline intrusive rock was collected from the *ca*. 26–28 Ma La Sal Mountain intrusive complex (Hunt 1958) approximately 15 km south of sample 171-01 and at an elevation approximately equal to the top of the canyon rim above 171-01.

Apatite fission track and U–Pb data

Both of these samples offer significant challenges for apatite fission track data collection. Sample 171-01 contains abundant euhedral to highly rounded detrital apatite grains. Some grains contain abundant natural fission tracks and these grains are usually characterized by large Dpar values (>2.5 µm) and commonly these grains exhibit minor rounding. Some grains contain very few or no fission tracks. These grains usually exhibit small Dpar values (<2.0 µm) although some high Dpar grains containing abundant etched defects are also present. Most of the small Dpar grains exhibit significant rounding. Sample 171-03 contains abundant large, euhedral apatite grains. Most of these grains contain abundant etched defects and it is often quite difficult to distinguish these defects from natural fission tracks. This igneous sample yields a pooled fission track age of 31.2 ±4 Ma. As will be seen below, the pooled fission track age of ~44 Ma for sedimentary sample 171-01 is meaningless as it represents a mixture of young ages (due to total annealing of fast annealing apatite fission tracks by the La Sal Mountain intrusive event) and old ages (due to preservation of slow annealing apatite fission tracks that predate the La Sal Mountain intrusive event).

The combination of fission track age and length data and U–Pb data for sample 171-01 (Figures 12-2 to 12-7) permits a detailed assessment of the thermal history of this sedimentary sample to be undertaken. Figure 12-2 illustrates the distributions of apatite $^{206}Pb/^{238}U$ age and U–Pb zircon age for sample 171-01. The apatite $^{206}Pb/^{238}U$ age data define two broad populations at ~0.5 and 1.45 Ga with a minor peak at 0.9 Ga. Figure 12-3 shows the relationship between apatite fission track age and apatite $^{206}Pb/^{238}U$ age for the same detrital grains. The two major apatite $^{206}Pb/^{238}U$ age populations can be correlated with discrete apatite fission track age populations, with the apatite grains characterized by old (*ca*. 1.45 Ga) $^{206}Pb/^{238}U$ ages yielding young (<150 Ma) fission track ages, and the apatite grains characterized by younger (*ca*. 0.5 Ga) $^{206}Pb/^{238}U$ ages yielding older fission track ages between 100 and 300 Ma. Likewise the two major apatite $^{206}Pb/^{238}U$ age populations can be correlated with discrete Dpar populations (Figure 12-4), with the *ca*. 1.45 Ga $^{206}Pb/^{238}U$ age population yielding Dpar values which cluster between 1.5 and 2.5 µm, and the *ca*. 0.5 Ga $^{206}Pb/^{238}U$ age population yielding Dpar values which cluster between 2.5 and 3.5 µm. Figures 12-5 and 12-6 illustrate Dpar versus apatite fission track age and track length respectively. The oldest apatite fission track ages (c. 300 Ma) are in general characterized by the highest Dpar values of around 3.5 µm. Plots of apatite $^{206}Pb/^{238}U$ age (or fission track age) *versus* chemical

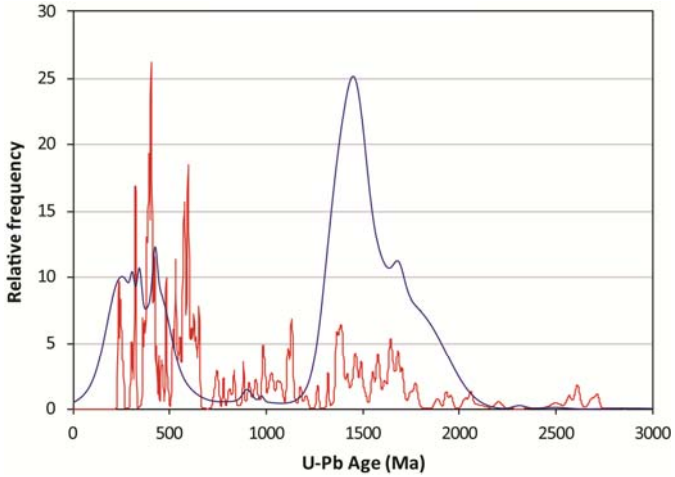

FIGURE 12-2. Distribution of apatite ^{207}Pb-corrected $^{206}Pb/^{238}U$ ages (blue) and U–Pb zircon ages (red) for sample 171-01.

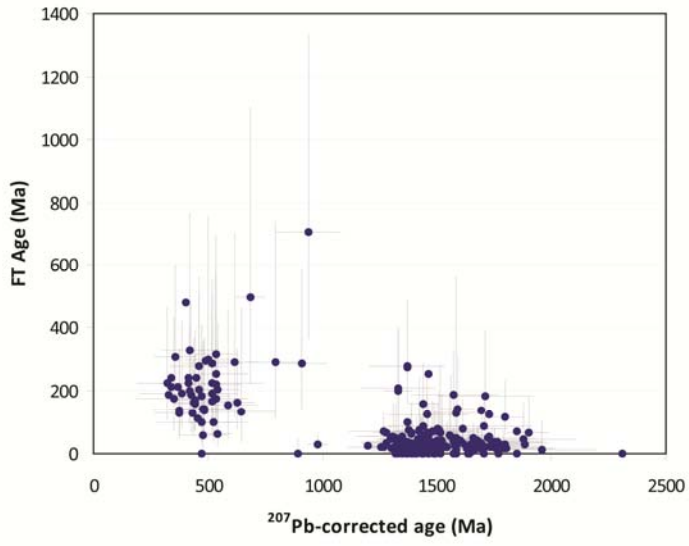

FIGURE 12-3. Apatite fission track age versus apatite ^{207}Pb-corrected $^{206}Pb/^{238}U$ age for sample 171-01.

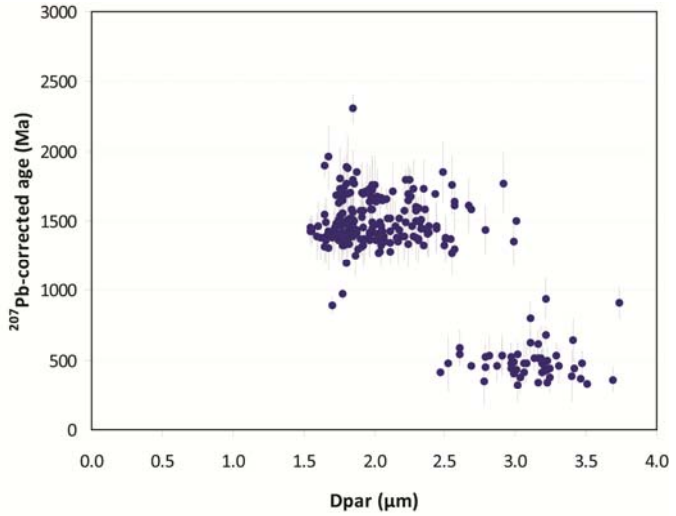

FIGURE 12-4. Apatite ^{207}Pb-corrected $^{206}Pb/^{238}U$ age versus Dpar for sample 171-01.

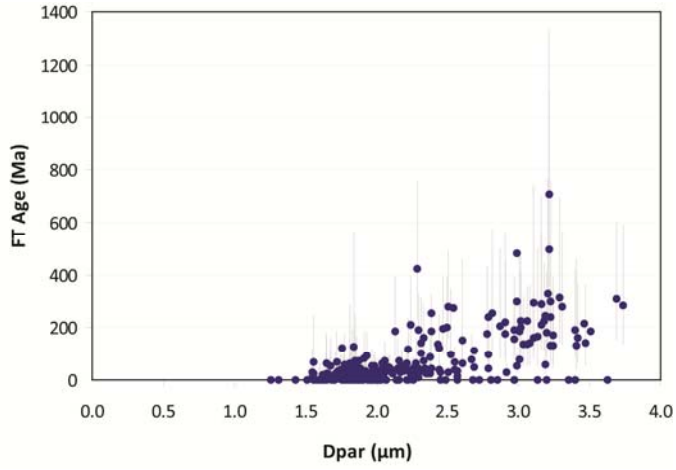

FIGURE 12-5. Apatite fission track age versus Dpar for sample 171-01.

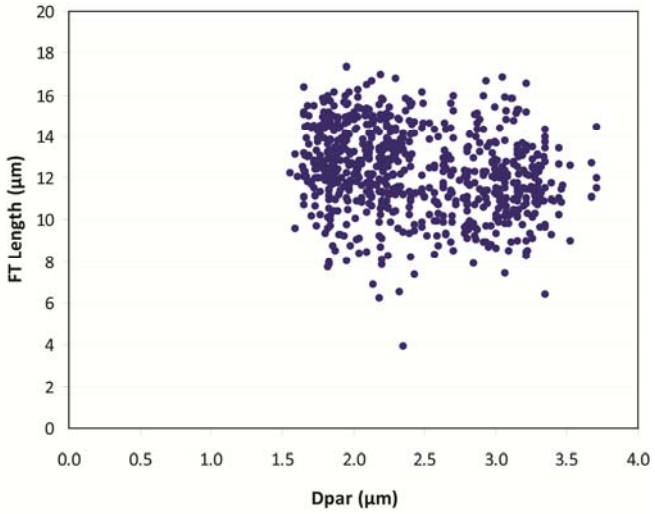

FIGURE 12-6. Apatite fission track length versus Dpar for sample 171-01.

composition variables (*e.g.*, Fe or La) also demonstrate that there are two discrete detrital apatite populations present in this sedimentary sample. These plots serve as a basis to split the apatite fission track data into discrete groups that can then be modeled separately using software for the inverse modeling of low-temperature thermochronometric data (*e.g.*, HeFTy, Ketcham 2005).

Thermal history analysis using HeFTy

Figure 12-7 shows the *Time–Temperature History* window in HeFTy containing the results of an inversion that successfully found 1000 acceptable thermal histories at the 95% confidence level. The resulting temperature–time history needs to be considered in conjunction with the available geological data. The La Sal Mountains alkaline intrusive complex was intruded at 26–28 Ma, which is consistent with the pooled fission track age of 31.2 ±4 Ma from 171-03 (the alkaline intrusive rock sample). In the sedimentary sample from Castle Valley (171-01), old (*i.e.*, Precambrian ^{207}Pb-corrected ^{206}Pb/^{238}U ages) detrital apatite grains show systematically young apatite fission track ages (Figure 12-3). These same detrital apatite grains yield small Dpar values (Figure 12-4) and are characterized by low Fe contents (not shown). This detrital apatite population exhibits a pooled fission track age of 26.4 ±2.5 Ma, similar in age to the timing of the La Sal Mountain intrusive event. The fission track age and length data modeled in Figure 12-7 is derived from the younger (*i.e.*, Paleozoic ^{207}Pb-corrected ^{206}Pb/^{238}U ages) detrital apatite population of sample 171-01. This detrital population exhibits larger Dpar values (Figure 12-4), higher Fe contents (not shown) and older fission track grain ages (Figure 12-3) which date back to the depositional age of sample 171-01 (Late to Middle Triassic). This detrital population constrains the peak temperature experienced by sample 171-01 during the La Sal Mountains intrusive event. The peak temperature is estimated at between 95–120°C (Figure 12-7), which was sufficient to totally anneal fission tracks in the detrital apatite population characterized by small Dpar values, yet only partially annealed fission tracks in the detrital apatite population characterized by high Dpar values.

CONCLUSIONS

Like zircon, apatite is a virtually ubiquitous component in clastic sedimentary rocks. It can yield reliable U–Pb age information once challenges are overcome with respect to low U and radiogenic Pb concentrations and elevated common Pb to radiogenic Pb ratios, and potential approaches optimized for quadrupole or rapid-scanning magnetic-sector LA–ICP–MS systems are outlined in this chapter. Apatite offers several key advantages when compared to zircon in sedimentary provenance analysis. It is more likely to represent first cycle detritus as it is mechanically less stable than zircon and is chemically unstable in weathering profiles, particularly in the presence of low pH meteoric water. Unlike zircon which is generally restricted to igneous rocks of felsic composition, apatite is a nearly ubiquitous accessory phase in igneous rocks of both felsic and mafic composition. Unlike zircon, the trace element composition of igneous apatite is a useful diagnostic tool in igneous petrogenesis studies as trace element partition coefficients in igneous apatite are typically

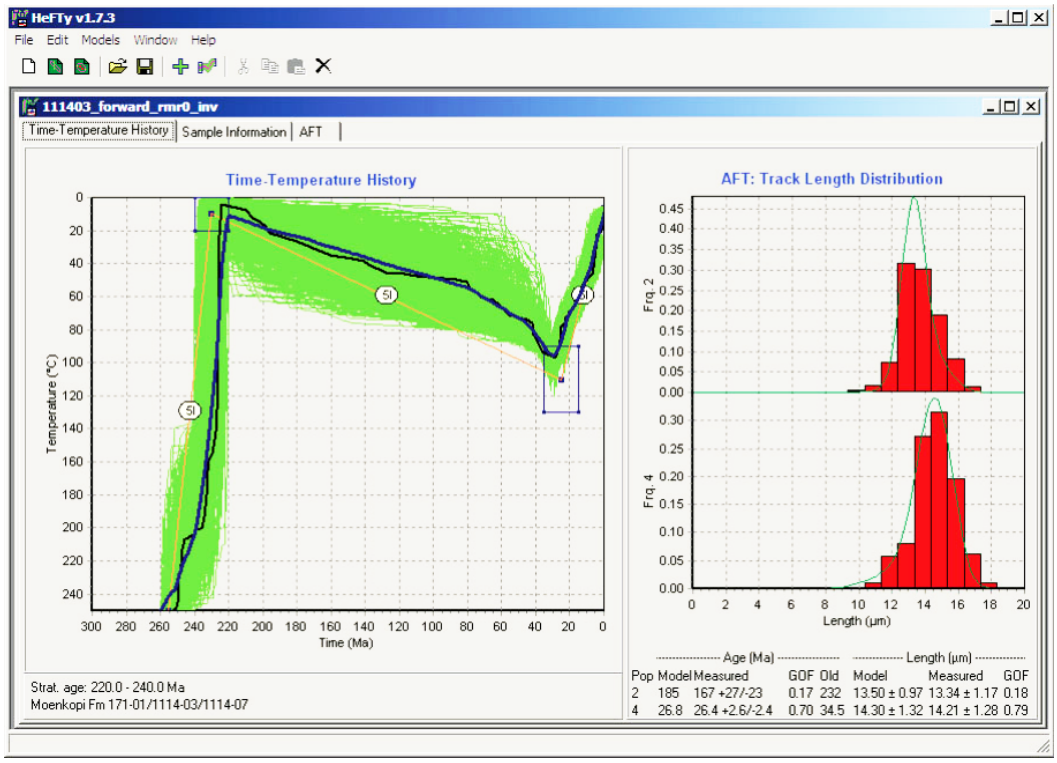

FIGURE 12-7. The *Time-Temperature History* window in HeFTy showing inversion results comprised of 1000 acceptable models at the 95% confidence level.

very sensitive to changes in magmatic conditions. The trace element chemistry of detrital apatite can therefore provide an effective link to the parent igneous rock type.

Integrating apatite fission track and U–Pb dating using the LA–ICP–MS method has many potential applications in sedimentary provenance analysis. U–Pb data provide information on the high temperature thermal history of the igneous source while the apatite fission track data yield constraints on the low temperature thermal history of the source region in detrital samples which have remained below the temperature of the apatite PAZ (60 to 110°C) since deposition. In detrital samples that were heated above the temperature of the apatite PAZ following deposition, then the fission track data yield constraints on the thermal history of the host sedimentary rock. U–Pb age data also place useful constraints on the time window over which fission track thermal history modeling should be considered and can help identify the presence of diagenetic or contaminant apatite grains. U–Pb and apatite trace element data may also prove useful for characterizing and distinguishing between discrete detrital apatite populations (which may have different annealing kinetics).

Future research avenues in apatite provenance and thermochronology studies by LA–ICP–MS include the application of apatite trace element data as either a provenance tool or in quantifying fission track annealing kinetics. Presently the lack of a comprehensive database on apatite compositions in potential source rocks remains a stumbling block to routine provenance studies using apatite trace element geochemistry (*cf*. Morton & Yaxley 2007) and this problem is particularly acute for apatite of metamorphic origin. Minor and trace element concentrations in apatite are very important for characterizing the thermal annealing kinetics of fission tracks in apatite. Chlorine typically exerts the dominant control on apatite structure, but unfortunately it is difficult to analyze by ICP–MS due to its high first ionization potential. Reliable apatite chlorine concentration measurements by ICP–MS would remove the need for additional EPMA analyses and would enable the apatite fission track and U–Pb dating protocol described in this chapter to be integrated with key information on apatite thermal annealing kinetics.

ACKNOWLEDGEMENTS

DMC thanks Paul Sylvester and Mike Tubrett (Memorial University, St. John's), Shane Tyrrell and Stephen Daly (University College Dublin), Balz Kamber (Trinity College Dublin) and Richard Spikings (University of Geneva) for assistance and advice on undertaking U–Pb apatite dating by LA–ICP–MS. Tom Culligan (University College Dublin) is thanked for apatite grain mount preparation. RAD thanks Paul O'Sullivan, Margaret Donelick (both at Apatite to Zircon, Inc.) and Charles Knaack (Washington State University) for years of discussions regarding LA–ICP–MS approaches, Margaret Donelick for providing the LA–ICP–MS data, Greg Arehart (University of Nevada–Reno) for performing the ^{252}Cf irradiations, Stuart Thomson for advice on using McClure Mountain apatite as a reference material and Ken Severin (University of Alaska–Fairbanks) for providing detailed EPMA data for Durango apatite. Bryan Sell and Stuart Thomson are thanked for careful and constructive reviews which significantly improved this manuscript.

REFERENCES

AMELIN, Y. & ZAITSEV, A. N. (2002): Precise geochronology of phoscorites and carbonatites: The critical role of U-series disequilibrium in age interpretations. *Geochim. Cosmochim. Ac.* **66**, 2399-2419.

BARBARAND, J., CARTER, A., WOOD, I. & HURFORD, T. (2003): Compositional and structural control of fission-track annealing in apatite. *Chem. Geol.* **198**, 107-137.

BARFOD, G. H., OTERO, O. & ALBARÈDE, F. (2003): Phosphate Lu-Hf geochronology. *Chem. Geol.* **200**, 241-253.

BELOUSOVA, E.A., GRIFFIN, W.L., O'REILLY, S.Y. & FISHER, N.I. (2002): Apatite as an indicator mineral for mineral exploration: trace-element compositions and their relationship to host rock type. *J. Geochem. Explor.* **76**, 45-69.

BERNET, M. & SPIEGEL, C. (2004): Introduction: Detrital thermochronology. *Geological Society of America Special Paper* **378**, 1-6.

CAMPBELL, I.H., REINERS, P.W., ALLEN, C.M., NICOLESCU, S. & UPADHYAY, R. (2005): He–Pb double dating of detrital zircons from the Ganges and Indus Rivers: Implication for quantifying sediment recycling and provenance studies. *Earth Planet. Sc. Lett.* **237**, 402-432.

CARLSON, W.D., DONELICK, R.A. & KETCHAM, R.A. (1999): Variability of apatite fission-track annealing kinetics: I. Experimental results. *Am. Mineral.* **84**, 1213-1223.

CARRAPA, B., DECELLES, P.G., REINERS, P.W., GEHRELS, G.E. & SUDO, M. (2009): Apatite triple dating and white mica ^{40}Ar/^{39}Ar thermochronology of syntectonic detritus in the Central Andes: A multiphase tectonothermal history. *Geology* **37**, 407-410.

CHAMBERLAIN, K.R. & BOWRING, S.A. (2000): Apatite-feldspar U–Pb thermochronometer: A reliable, mid-range (450°C), diffusion-controlled system. *Chem. Geol.* **172**, 173-200.

CHANG, Z.S., VERVOORT, J.D., MCCLELLAND, W.C. & KNAACK, C. (2006): U–Pb dating of zircon by LA-ICP-MS. *Geochem. Geophys. Geosyst.* **7**.

CHEW, D. M., SYLVESTER, P. J. & TUBRETT, M. N. (2011): U–Pb and Th-Pb dating of apatite by LA–ICP–MS. *Chem. Geol.* **280**, 200-216.

COCHERIE, A. (2009): Common-Pb correction in laser U–Pb geochronology using MC-ICP–MS and a multi-ion counting system. *Geochim. Cosmochim. Ac.* **73**, A233-A233.

COCHERIE, A., FANNING, C.M., JEZEQUEL, P. & ROBERTA, M. (2009): LA-MC-ICP–MS and SHRIMP U–Pb dating of complex zircons from Quaternary tephras from the French Massif Central: Magma residence time and geochemical implications. *Geochim. Cosmochim. Ac.* **73**, 1095-1108.

COX, R.A. & WILTON, D.H.C. (2006): U–Pb dating of perovskite by LA-ICP-MS: An example from the Oka carbonatite, Quebec, Canada. *Chem. Geol.* **235**, 21-32.

DICKINSON, W.R. & GEHRELS, G.E. (2009): Use of U–Pb ages of detrital zircons to infer maximum depositional ages of strata: A test against a Colorado Plateau Mesozoic database. *Earth Planet. Sc. Lett.* **288**, 115-125.

DILL, H.G. (1994): Can REE Patterns and U-Th Variations be used as a tool to determine the origin of apatite in clastic rocks? *Sediment. Geol.* **92**, 175-196.

DONELICK, R.A. (1993): A method of fission track analysis utilizing bulk chemical etching of

apatite. U.S. Patent Number 5267274.

DONELICK, R.A., O'SULLIVAN, P.B. & KETCHAM, R.A. (2005): Apatite fission-track analysis. In: Reiners, P. W. & Ehlers, T. A. (eds.) *Low-Temperature Thermochronology: Techniques, Interpretations, and Applications*: Rev. Mineral. Geochem., **58**, 49-94.

EGGINS, S.M., KINSLEY, L.P.J. & SHELLEY, J.M.G. (1998): Deposition and element fractionation processes during atmospheric pressure laser sampling for analysis by ICP-MS. *Appl. Surf. Sci,* **127**, 278-286.

FARLEY, K.A. (2000): Helium diffusion from apatite: General behavior as illustrated by Durango fluorapatite. *J Geophys. Res.* **105**, 2903-2914.

FLEISCHER, R.L., PRICE, P.B. & WALKER, R.M. (1975): *Nuclear tracks in solids: Principles and applications*: University of California Press, Berkeley.

FOSTER, G.L. & VANCE, D. (2006): In situ Nd isotopic analysis of geological materials by laser ablation MC-ICP-MS. *J. Anal. Atom. Spectrom.* **21**, 288-296.

GALLAGHER, K. (1995): Evolving temperature histories from apatite fission-track data. *Earth Planet. Sc. Lett.* **136**, 421-435.

GALLAGHER, K., BROWN, R. & JOHNSON, C. (1998): Fission track analysis and its applications to geological problems. *Annu. Rev. Earth Pl. Sc.* **26**, 519-572.

GEHRELS, G.E., VALENCIA, V.A. & RUIZ, J. (2008): Enhanced precision, accuracy, efficiency, and spatial resolution of U–Pb ages by laser ablation-multicollector-inductively coupled plasma-mass spectrometry. *Geochem. Geophys. Geosyst.* **9**.

GIBSON, G.M. & IRELAND, T.R. (1996): Extension of Delamerian (Ross) orogen into western New Zealand: Evidence from zircon ages and implications for crustal growth along the Pacific margin of Gondwana. *Geology* **24**, 1087-1090.

GLEADOW, A.J.W. (1981): Fission-track dating methods - what are the real alternatives. *Nucl. Tracks Rad. Meas.* **5**, 3-14.

GLEADOW, A.J.W., DUDDY, I.R., GREEN, P.F. & HEGARTY, K.A. (1986a): Fission-track lengths in the apatite annealing zone and the interpretation of mixed ages. *Earth Planet. Sc. Lett.* **78**, 245-254.

GLEADOW, A.J.W., DUDDY, I.R., GREEN, P.F. & LOVERING, J.F. (1986b): Confined fission-track lengths in apatite - a diagnostic-tool for thermal history analysis. *Contrib. Mineral. Petr.* **94**, 405-415.

GLEADOW, A.J.W., GLEADOW, S.J., BELTON, D.X., KOHN, B.P., KROCHMAL, M.S. & BROWN, R.W. (2009): Coincidence mapping - a key strategy for the automatic counting of fission tracks in natural minerals. *Geol. Soc. Spec. Publ.* **324**, 25-36.

GREEN, P.F. (1988): The Relationship between Track Shortening and Fission-Track Age Reduction in Apatite - Combined Influences of Inherent Instability, Annealing Anisotropy, Length Bias and System Calibration. *Earth Planet. Sc. Lett.* **89**, 335-352.

GREEN, P.F., DUDDY, I.R., GLEADOW, A.J.W., TINGATE, P.R. & LASLETT, G.M. (1985): Fission-track annealing in apatite-track length measurements and the form of the Arrhenius plot. *Nucl. Tracks Rad. Meas.* **10**, 323-328.

GREEN, P.F., DUDDY, I.R., GLEADOW, A.J.W., TINGATE, P.R. & LASLETT, G.M. (1986): Thermal annealing of fission tracks in apatite.1. A qualitative description. *Chem. Geol.* **59**, 237-253.

GREGORY, C.J., MCFARLANE, C.R.M., HERMANN, J. & RUBATTO, D. (2009): Tracing the evolution of calc-alkaline magmas: In-situ Sm-Nd isotope studies of accessory minerals in the Bergell Igneous Complex, Italy. *Chem. Geol.* **260**, 73-86.

GREGORY, C.J., RUBATTO, D., ALLEN, C.M., WILLIAMS, I.S., HERMANN, J. & IRELAND, T. (2007): Allanite micro-geochronology: A LA-ICP-MS and SHRIMP U-Th-Pb study. *Chem. Geol.* **245**, 162-182.

HASEBE, N., BARBARAND, J., JARVIS, K., CARTER, A. & HURFORD, A. J. (2004): Apatite fission-track chronometry using laser ablation ICP-MS. *Chem. Geol.* **207**, 135-145.

HASEBE, N., CARTER, A., HURFORD, A.J. & ARAI, S. (2009): The effect of chemical etching on LA–ICP-MS analysis in determining uranium concentration for fission-track chronometry. In: Lisker, F., Ventura, B. & Glasmacher, U. A. (eds.) *Thermochronological methods; from palaeotemperature constraints to landscape*

evolution models: Geol. Soc. Spec. Publ., **324**, 37-46.

HENDRIKS, B.W.H. & REDFIELD, T.F. (2005): Apatite fission track and (U-Th)/He data from Fennoscandia: An example of underestimation of fission track annealing in apatite. *Earth Planet. Sc. Lett.* **236**, 443-458.

HOSKIN, P.W.O. & SCHALTEGGER, U. (2003): The composition of zircon and igneous and metamorphic petrogenesis. In: Hanchar, J. M. & Hoskin, P. W. O. (eds.) *Zircon*: Rev. Mineral. Geochem., **53**, 27-62.

HUNT, C. B. (1958). Structural and igneous geology of the La Sal Mountains, Utah. *U.S. Geoloogical Survey Professional Paper* **294-I**, 305-364.

HURFORD, A.J. & GREEN, P.F. (1982): A user's guide to fission-track dating calibration. *Earth Planet. Sc. Lett.* **59**, 343-354.

HURFORD, A.J. & GREEN, P.F. (1983): The zeta-age calibration of fission-track dating. *Isotope Geoscience* **1**, 285-317.

JACKSON, S.E., LONGERICH, H.P., HORN, I. & DUNNING, G.R. (1996): The application of laser ablation microprobe (LAM)-ICP-MS to in situ U–Pb zircon geochronology. *J.Conf.Abs.* **1**, 283.

JENNINGS, E.S., MARSCHALL, H.R., HAWKESWORTH C.J. & STOREY, C.D. (2011): Characterization of magma from inclusions in zircon: Apatite and biotite work well, feldspar less so. *Geology* **39**, 863-866.

KETCHAM, R.A. (2005): Forward and inverse modeling of low-temperature thermochronometry data. In: Reiners, P. W. & Ehlers, T. A. (eds.) *Low-Temperature Thermochronology: Techniques, Interpretations, and Applications*: Rev. Mineral. Geochem., **58**, 275-314.

KINNY, P.D. & MAAS, R. (2003): Lu-Hf and Sm-Nd isotope systems in zircon. In: Hanchar, J. M. & Hoskin, P. W. O. (eds.) *Zircon*: Rev. Mineral. Geochem., **53**, 327-341.

KOŠLER, J. & SYLVESTER, P.J. (2003): Present trends and the future of zircon in geochronology: laser ablation ICP–MS. In: Hanchar, J. M. & Hoskin, P. W. O. (eds.) *Zircon*: Rev. Mineral. Geochem., **53**, 243-275.

KOŠLER, J., FONNELAND, H., SYLVESTER, P., TUBRETT, M. & PEDERSEN, R.B. (2002): U–Pb dating of detrital zircons for sediment provenance studies - a comparison of laser ablation ICP–MS and SIMS techniques. *Chem. Geol.* **182**, 605-618.

KOŠLER, J., TUBRETT, M.N. & SYLVESTER, P.J. (2001): Application of laser ablation ICP-MS to U-Th-Pb dating of monazite. *Geostandard. Newslett.* **25**, 375-386.

KUIPER, K.F., DEINO, A., HILGEN, F.J., KRIJGSMAN, W., RENNE, P.R. & WIJBRANS, J.R. (2008): Synchronizing rock clocks of Earth history. *Science* **320**, 500-504.

LASLETT, G.M., GREEN, P.F., DUDDY, I.R. & GLEADOW, A.J.W. (1987): Thermal annealing of fission tracks in apatite. II: A quantitative analysis. *Chem. Geol.* **65**, 1-3.

LUDWIG, K.R. (1998): On the treatment of concordant uranium-lead ages. *Geochim. Cosmochim. Acta* **62**, 665-676.

MANK, A.J.G. & MASON, P.R.D. (1999): A critical assessment of laser ablation ICP-MS as an analytical tool for depth analysis in silica-based glass samples. *J. Anal. Atom. Spectrom.* **14**, 1143-1153.

MCDOWELL, F.W., MCINTOSH, W.C. & FARLEY, K.A. (2005): A precise ^{40}Ar-^{39}Ar reference age for the Durango apatite (U-Th)/He and fission-track dating standard. *Chem. Geol.* **214**, 249-263.

MORTON, A.C. & HALLSWORTH, CR. (1999): Processes controlling the composition of heavy mineral assemblages in sandstones. *Sediment. Geol.* **124**, 3-29.

MORTON, A. & YAXLEY, G. (2007): Detrital apatite geochemistry and its application in provenance studies. In: Arribas, J., Critelli, S. & Johnsson, M. J. (eds.) *Sedimentary Provenance and Petrogenesis: Perspectives from Petrography and Geochemistry:* Geol. Soc. Amer. Spec. Pap. **420** 319–344.

NORMAN, M.D., PEARSON, N.J., SHARMA, A. & GRIFFIN, W.L. (1996): Quantitative analysis of trace elements in geological materials by laser ablation ICP–MS: Instrumental operating conditions and calibration values of NIST glasses. *Geostandard. Newslett.* **20**, 247-261.

PATON, C., HELLSTROM, J., PAUL, B., WOODHEAD, J. & HERGT, J. (2011): Iolite: Freeware for the visualisation and processing of mass spectrometric data. *J. Anal. Atom. Spectrom.* **26**, 2508-2518.

PATON, C., WOODHEAD, J. D., HELLSTROM, J.C., HERGT, J. M., GREIG, A. & MAAS, R. (2010): Improved laser ablation U–Pb zircon geochronology through robust downhole fractionation correction. *Geochem. Geophys. Geosyst.* **11**.

PETRUS, J.A. & KAMBER, B.S. (in press): VizualAge: a novel approach to LA-ICP-MS U–Pb geochronology. *Geostand. Geoanal. Res.*

PICCOLI, P.M. & CANDELA, P.A. (2002): Apatite in igneous systems. In: Kohn, M. L., Rakovan, J. & Hughes, J. M. (eds.) *Phosphates: Geochemical, Geobiological and Materials Importance*: Rev. Mineral. Geochem., **48**, 255-292.

PRICE, P.B. & WALKER, R.M. (1962): Chemical Etching of Charged-Particle Tracks in Solids. *Journal of Appl. Phys.* **33**, 3407-3412.

PRICE, P.B. & WALKER, R.M. (1963): Fossil Tracks of Charged Particles in Mica and Age of Minerals. *J Geophys. Res.* **68**, 4847-4862.

RENNE, P.R., SWISHER, C.C., DEINO, A.L., KARNER, D.B., OWENS, T.L. & DEPAOLO, D.J. (1998): Intercalibration of standards, absolute ages and uncertainties in $^{40}Ar/^{39}Ar$ dating. *Chem. Geol.* **145**, 117-152.

RØNSBO, J.G. (1989): Coupled substitutions involving REEs and Na and Si in apatites in alkaline rocks from the Ilimaussaq intrusion, South-Greenland, and the petrological implications. *Am. Mineral.* **74**, 896-901.

SCHMITZ, M.D., BOWRING, S.A. & IRELAND, T.R. (2003): Evaluation of Duluth Complex anorthositic series (AS3) zircon as a U–Pb geochronological standard: New high-precision isotope dilution thermal ionization mass spectrometry results. *Geochim. Cosmochim. Ac.* **67**, 3665-3672.

SCHOENE, B. & BOWRING, S.A. (2006): U–Pb systematics of the McClure Mountain syenite: thermochronological constraints on the age of the Ar-40/Ar-39 standard MMhb. *Contrib. Mineral. Petr.* **151**, 615-630.

SCHOENE, B. & BOWRING, S.A. (2007): Determining accurate temperature-time paths from U–Pb thermochronology: An example from the Kaapvaal craton, southern Africa. *Geochim. Cosmochim. Acta* **71**, 165-185.

SCHOENE, B., LATKOCZY, C., SCHALTEGGER, U. & GÜNTHER, D. (2010): A new method integrating high-precision U–Pb geochronology with zircon trace element analysis (U–Pb TIMS-TEA). *Geochimica et Cosmochimica Acta* **74**, 7144–7159.

SELL, B.K. & SAMSON, S.D. (2011): A tephrochronologic method based on apatite trace-element chemistry. *Quaternary Res.* **76**, 157-166.

SHA, L.K. & CHAPPELL, B.W. (1999): Apatite chemical composition, determined by electron microprobe and laser-ablation inductively coupled plasma mass spectrometry, as a probe into granite petrogenesis. *Geochim. Cosmochim. Ac.* **63**, 3861-3881.

SIMONETTI, A., HEAMAN, L.M., CHACKO, T. & BANERJEE, N.R. (2006): In situ petrographic thin section U–Pb dating of zircon, monazite, and titanite using laser ablation-MC-ICP-MS. *Int. J. Mass. Spectrom.* **53**, 87-97.

SPEAR, F.S. & PYLE, J.M. (2002): Apatite, monazite, and xenotime in metamorphic rocks. In: Kohn, M.L., Rakovan, J. & Hughes, J.M. (eds.) *Phosphates: Geochemical, Geobiological and Materials Importance*: Rev. Mineral. Geochem., **48**, 293-336.

STACEY, J.S. & KRAMERS, J.D. (1975): Approximation of terrestrial lead isotope evolution by a two-stage model. *Earth Planet. Sc. Lett.* **26**, 207-221.

STEIGER, R.H. & JÄGER, E. (1977): Subcommission on geochronology: Convention on the use of decay constants in geo- and cosmochronology. *Earth Planet. Sc. Lett.* **36**, 359-362.

STOREY, C.D., SMITH, M.P. & JEFFRIES, T.E. (2007): In situ LA-ICP-MS U–Pb dating of metavolcanics of Norrbotten, Sweden: Records of extended geological histories in complex titanite grains. *Chem. Geol.* **240**, 163-181.

SYLVESTER, P.J. & GHADERI, M. (1997): Trace element analysis of scheelite by excimer laser ablation inductively coupled plasma mass spectrometry (ELA-ICP-MS) using a synthetic silicate glass standard. *Chem. Geol.* **141**, 49-65.

THOMSON, S.N., GEHRELS, G.E., RUIZ, J. & BUCHWALDT, R. (2012): Routine low-damage apatite U–Pb dating using laser ablation-multicollector-ICP–MS. *Geochem. Geophys.*

Geosyst. **13**, Q0AA21, doi:10.1029/2011GC003928.

WILLIAMS, I.S. (1998): U-Th-Pb geochronology by ion microprobe. In: McKibben, M.A., Shanks III, W.C. & Ridley, W.I. (eds.) *Applications of microanalytical techniques to understanding mineralizing processes*: Rev. Econ. Geol., 1–35.

WILLIGERS, B.J.A., BAKER, J.A., KROGSTAD, E.J. & PEATE, D.W. (2002): Precise and accurate in situ Pb-Pb dating of apatite, monazite, and sphene by laser ablation multiple-collector ICP-MS. *Geochim. Cosmochim. Ac.* **66**, 1051-1066.

APPENDIX

General ICP–MS Data Modeling (FTUPbICP)

Background values (in cps) for all isotopes were calculated for each LA–ICP–MS spot analysis using the following protocol: a) the background value was assigned as the scan closest to the global minima for ^{43}Ca and ^{238}U (if no such global minima was found, the analysis was deemed a failure), b) a best-fit line was fitted to the background signals by chi-squared minimization, outliers identified, and a best-fit line again fitted to the data excluding the outliers, c) for a best-fit line exhibiting a negative slope (*i.e.*, decreasing background with time), the last background scan was assigned as the background value; for a best-fit line exhibiting a zero or positive slope, the mean value (excluding outliers) was assigned as the background value, and d) the error of the background value was set equal to the standard deviation of the data about either their best-fit line or mean. Individual isotope signal values (units of cps) were modeled by fitting a sum of ≤10 Gaussian equations to the raw signal data (including background) using chi-squared minimization. Two fitting passes were performed: after the first pass, all raw signal values greater than two standard deviations away from the sum of the fitted Gaussian equations were designated as outliers; on the second pass the software fits a sum of Gaussian equations to the data excluding the outliers. For each scan, the signal value was calculated by subtracting the background value from the fitted raw signal value. After the second pass, the standard deviation of the data (including outliers) about their respective sum of fitted Gaussian equations was taken as the absolute error ($\sigma_{isotope}$) for each data scan. The error of the sum of N background-corrected signal values for a particular isotope was taken as the product of $N^{1/2} * \sigma_{isotope}$.

ICP–MS data modeling (fission track and U–Pb data)

Durango apatite was used as the apatite fission track zeta age calibration standard (Table 12-2). For fission track dating of unknowns, LA–ICP–MS U concentration measurements were also undertaken on 50 spots of Durango apatite (employing specific spots from the primary zeta calibration session) to calibrate ^{238}U/^{43}Ca. Fission track ages were calculated using the scheme presented by Donelick *et al*. (2005) using a zeta calibration approach modified from Hurford & Green (1983) and Hasebe *et al*. (2004). The ^{238}U/^{43}Ca ratio for each data scan was calculated using the background-corrected, sum-of-Gaussian-fitted signal values for the two isotopes. Each data scan was treated as a "slice" of ablated mineral where: a) the thickness of the slice was determined by the ^{43}Ca value multiplied by a calibration factor in terms of microns per ^{43}Ca, and b) the ablation depth of the slice was determined by the sum of the thicknesses of the overlying slices plus one half of the thickness of the current slice. A weighted mean ^{238}U/^{43}Ca ratio was calculated for each spot by summing the ^{238}U/^{43}Ca ratio values for each slice weighted by: a) slice thickness and b) slice depth accounting for the likelihood that fission tracks emanating from that depth with intersect the polished and etched mineral surface. Below $l_o/2$ (l_o taken as the mean length of natural Durango confined track lengths), the likelihood of ^{238}U contributing fission tracks to the etched apatite surface is effectively zero. The error of the weighted mean ^{238}U/^{43}Ca ratio was calculated as follows:

$$\left(\frac{^{238}U}{^{43}Ca}\right)_{\sigma} = \left(\left(\frac{N\sigma_{^{43}Ca}}{\sum {}^{43}Ca}\right)^2 + \left(\frac{N\sigma_{^{238}U}}{\sum {}^{238}U}\right)^2\right)^{1/2} \left(\frac{^{238}U}{^{43}Ca}\right) \qquad \text{(A1)}$$

Where N = number of data scans used to calculate weighted mean (^{238}U/^{43}Ca)
Σ^{43}Ca = sum of ^{43}Ca background corrected signal values above a depth of $l_o/2$
Σ^{238}U = sum of ^{238}U background corrected signal values above a depth of $l_o/2$.

Apatite U–Pb age standards analyzed in this study are described in the main text of this chapter. Two primary and two secondary standard spots were analyzed prior to and following each group of ~25–40 unknown sample spots. Up to 10 spots of each tertiary standard were analyzed near the beginning and the end of analytical sessions. The approach to correcting for elemental fractionation in this study avoids any assumption of linearly varying isotopic ratios with time, which has been made in several U–Pb zircon studies (*e.g.*, Chang *et al.* 2006). Instead, individual isotopes are modeled and background-corrected signal data and their errors are calculated for each data scan as described above. Time-integrated fractionation factors were determined for each primary standard spot analysis based on this background-corrected signal data. For any particular isotopic ratio (*e.g.*, ^{206}Pb/^{238}U), the fractionation factor equals the accepted isotopic ratio divided by the measured ratio. Fractionation factors were calculated based on the following assumptions: a) ^{235}U values were calculated from measured ^{238}U

values (Steiger & Jäger 1977), b) zero fractionation was assumed between ^{206}Pb and ^{207}Pb, and c) a ^{207}Pb-based common Pb correction was applied using the independently measured ^{207}Pb/^{206}Pb ratio of 0.881924 for McClure Mountain apatite common Pb (Schoene & Bowring 2006). The equations (A2–A4) for calculating the fractionation factors are listed below. These fractionation factors were then applied to the unknowns, whose common Pb isotopic composition was estimated using the Stacey & Kramer (1975) Pb evolution model. A ^{207}Pb-corrected ^{206}Pb/^{238}U age was calculated using a Pb isotopic composition calculated with the Stacey & Kramers (1975) model using an initial age estimate of the oldest age standard (1099 Ma). This ^{207}Pb-corrected age is then used to calculate a new Pb isotopic composition using the Stacey & Kramers (1975) model, an updated ^{207}Pb-corrected age is calculated and the process is repeated iteratively. Equations A5–A8 for calculating the ^{207}Pb-corrected age and its associated uncertainties are listed below.

Fractionation factors (Table 12-A1) were calculated using the following equations (* denotes radiogenic Pb; subscript *t* true values; subscript *m* indicates measured values based on background-corrected signals summed over *N* data scans):

$$f_{206} = \frac{\left(\frac{^{206*}Pb_t}{^{238}U_t}\right)}{\left(\frac{^{206*}Pb_m}{^{238}U_m}\right)} \quad \text{(A2a)} \qquad f_{207} = \frac{\left(\frac{^{207*}Pb_t}{^{235}U_t}\right)}{\left(\frac{^{207*}Pb_m}{^{235}U_m}\right)} \quad \text{(A2b)}$$

Fractionation factor errors were calculated using the following equations (σ indicates absolute error of a single data scan for its respective measured isotope):

$$\sigma_{f\,206} = f_{206}\left(\left(\frac{N^{1/2}\sigma_{206Pbm}}{^{206}Pb_m}\right)^2 + \left(\frac{N^{1/2}\sigma_{238Um}}{^{238}U_m}\right)^2\right)^{1/2} \quad \text{(A3a)}$$

$$\sigma_{f\,207} = f_{207}\left(\left(\frac{N^{1/2}\sigma_{207Pbm}}{^{207}Pb_m}\right)^2 + \left(\frac{N^{1/2}\sigma_{235Um}}{^{235}U_m}\right)^2\right)^{1/2} \quad \text{(A3b)}$$

Radiogenic Pb values may be written as follows (subscript *com* indicates common Pb):

$$^{206*}Pb_t = {}^{206}Pb_m - {}^{206}Pb_{com} \qquad ^{207*}Pb_t = {}^{207}Pb_m - {}^{206}Pb_{com}\left(\frac{^{207}Pb_{com}}{^{206}Pb_{com}}\right)$$

Substituting and solving for $^{206}Pb_{com}$ gives:

$$^{206}Pb_{com} = \frac{\frac{\left(^{206}Pb_m\left(\frac{^{207*}Pb_t}{^{235}U_t}\right)\right)}{^{238}U_m} - \frac{\left(^{207}Pb_m\left(\frac{^{206*}Pb_t}{^{238}U_t}\right)\right)}{^{235}U_m}}{\frac{\left(\frac{^{207*}Pb_t}{^{235}U_t}\right)}{^{238}U_m} - \frac{\left(\left(\frac{^{207}Pb_{com}}{^{206}Pb_{com}}\right)\left(\frac{^{206*}Pb_t}{^{238}U_t}\right)\right)}{^{235}U_m}} \quad \text{(A4)}$$

Common Pb corrected age and asymmetrical errors based on isotopic sums

The ^{207}Pb-corrected ^{206}Pb/^{238}U age (t_{Pbcom}) of each unknown spot analysis was calculated using a function *G* applied to the measured Pb and U isotope values (Table 12-A2):

$$t_{Pbcom} = G\left(f_{206}\,{}^{206}Pb_m,\, f_{207}\,{}^{207}Pb_m,\, {}^{238}U_m\right) \quad \text{(A5)}$$

Evaluation of *G* requires a $(^{207}Pb_{com}/^{206}Pb_{com})_{unk}$ value and evaluation of the amount of radiogenic Pb (* denotes radiogenic Pb). The value of $(^{207}Pb_{com}/^{206}Pb_{com})_{unk}$ was estimated using the Stacey & Kramer (1975) Pb evolution model as described earlier.

$$^{206*}Pb = f_{206}\,{}^{206}Pb_m - {}^{206}Pb_{com} \quad \text{(A6a)} \qquad ^{207*}Pb = f_{207}\,{}^{207}Pb_m - {}^{206}Pb_{com}\left(\frac{^{207}Pb_{com}}{^{206}Pb_{com}}\right)_{unk} \quad \text{(A6b)}$$

Six error components were calculated to estimate the asymmetrical negative and positive errors of t_{Pbcom}. These components were calculated as follows (measured isotope values based on background-corrected signals summed over *N* data scans):

$$-\sigma_{t206Pb} = t_{Pbcom} - G\left(\left(1 - N^{1/2}\left(\frac{\sigma_{206Pbm}}{^{206}Pb_m}\right)\right) f_{206}\,{}^{206}Pb_m,\, f_{207}\,{}^{207}Pb_m,\, {}^{238}U_m\right) \quad \text{(A7a)}$$

$$-\sigma_{t207Pb} = t_{Pbcom} - G\left(f_{206}\,{}^{206}Pb_m,\left(1 - N^{1/2}\left(\frac{\sigma_{207Pbm}}{^{207}Pb_m}\right)\right) f_{207}\,{}^{207}Pb_m,\, {}^{238}U_m\right) \quad \text{(A7b)}$$

$$-\sigma_{t238U} = t_{Pbcom} - G\left(f_{206}\,{}^{206}Pb_m,\, f_{207}\,{}^{207}Pb_m,\left(1 - N^{1/2}\left(\frac{\sigma_{238Um}}{^{238}U_m}\right)\right)^{238}U_m\right) \quad \text{(A7c)}$$

$$+\sigma_{t206Pb} = t_{Pbcom} - G\left(\left(1 + N^{1/2}\left(\frac{\sigma_{206Pbm}}{^{206}Pb_m}\right)\right) f_{206}\,{}^{206}Pb_m,\, f_{207}\,{}^{207}Pb_m,\, {}^{238}U_m\right) \quad \text{(A7d)}$$

$$+\sigma_{t207Pb} = t_{Pbcom} - G\left(f_{206}\,{}^{206}Pb_m,\left(1 + N^{1/2}\left(\frac{\sigma_{207Pbm}}{^{207}Pb_m}\right)\right) f_{207}\,{}^{207}Pb_m,\, {}^{238}U_m\right) \quad \text{(A7e)}$$

$$+\sigma_{t238U} = t_{Pbcom} - G\left(f_{206}\,{}^{206}Pb_m,\, f_{207}\,{}^{207}Pb_m,\left(1 + N^{1/2}\left(\frac{\sigma_{238Um}}{^{238}U_m}\right)\right)^{238}U_m\right) \quad \text{(A7f)}$$

The error on t_{Pbcom} is then calculated as follows:

$$-\sigma_{tPbcom} = \left(\left(-\sigma_{t206Pb}\right)^2 + \left(+\sigma_{t207Pb}\right)^2 + \left(+\sigma_{t238U}\right)^2\right)^{1/2} \quad \text{(A8a)}$$

$$+\sigma_{tPbcom} = \left(\left(-\sigma_{t207Pb}\right)^2 + \left(-\sigma_{t238U}\right)^2 + \left(+\sigma_{t206Pb}\right)^2\right)^{1/2} \quad \text{(A8b)}$$

The common Pb-corrected ages for the primary apatite age standard McClure Mountain (used to determine the fractionation factors listed in Table 12-A1) and the secondary apatite age standard Durango apatite are shown in Figures 12-1a and 12-b, respectively. Common Pb-corrected ages for selected spots from sample 171-01 are listed in Table 12-A2.

Table 12-A1. FRACTIONATION FACTORS AND ABSOLUTE ERRORS CALCULATED FOR PRIMARY STANDARD MCCLURE MOUNTAIN, SESSION AFTUPb111208-10

Session Spot Number	$^{206}Pb_m$	$^{207}Pb_m$	$^{235}U_m$	$^{238}U_m$	$N^{1/2}\sigma_{206Pbm}$	$N^{1/2}\sigma_{238Um}$	$^{206}Pb_{com}$ (Eqn. A4)	f_{206} (Eqn. A2a)	σ_{f206} (Eqn. A3a)
1	117698	29002	7698	1061371	923	10418	26929	0.990138	0.012441
2	68319	14778	5041	695114	869	7651	13136	1.066654	0.017942
35	60898	11781	4470	616366	659	8501	10021	1.025854	0.017989
36	38136	8996	2661	366857	467	4854	8239	1.039019	0.018737
59	49018	11689	3691	508926	539	5347	10742	1.125887	0.017123
60	55116	12038	4301	592995	535	8959	10738	1.131494	0.020323
88	39441	9167	3178	438119	337	5941	8355	1.193433	0.019122
89	33336	8186	2661	366954	581	4315	7592	1.206988	0.025367
117	48772	10496	4167	574494	500	9649	9313	1.232817	0.024252
118	53537	9194	5200	716920	465	9630	7398	1.315732	0.021047
151	40783	11232	3261	449693	649	6952	10766	1.268564	0.028154
152	59573	12845	5564	767155	826	9103	11405	1.348623	0.024604
185	50370	10541	4882	673138	651	5656	9254	1.386310	0.021369
186	63122	17436	5802	799945	838	5835	16726	1.459972	0.022121
214	42932	10372	4478	617386	435	6372	9571	1.567062	0.022675
215	31473	8732	2739	377719	529	6649	8387	1.385442	0.033717
243	41674	14409	3463	477475	468	8997	14559	1.491097	0.032701
244	46444	10962	4654	641725	442	7169	10042	1.492773	0.021909
272	36133	9122	3376	465512	410	5723	8532	1.428126	0.023903
273	40837	11441	3694	509392	655	5478	11016	1.446411	0.027944
297	26072	7950	2076	286257	380	6993	7817	1.327835	0.037766
298	47195	9288	4527	624215	446	6268	7958	1.347110	0.018581
326	23954	8248	2032	280187	380	4296	8326	1.518130	0.033517
327	35429	9077	3378	465820	454	6287	8527	1.466223	0.027296
355	47500	14251	4380	603935	345	6714	13958	1.524646	0.020245
356	53823	12914	5317	733083	531	7412	11892	1.480419	0.020916
390	73145	38801	4529	624507	960	7280	41947	1.695051	0.029749
423	29914	8600	2959	408052	244	5806	8336	1.601285	0.026269
424	28899	10243	2472	340797	448	4287	10401	1.560014	0.031136
452	61245	14613	6302	868954	550	9341	13432	1.538929	0.021561
453	36708	10398	3362	463521	574	6984	10041	1.471791	0.031964
481	36856	7883	3583	494059	528	7010	6978	1.400210	0.028224
482	43131	8204	3705	510791	409	9081	6927	1.194658	0.024075
510	38758	9211	3658	504359	514	9626	8456	1.409389	0.032761
511	60389	16142	5285	728671	628	8408	15347	1.369882	0.021279
537	32588	7857	3018	416102	382	5574	7246	1.390328	0.024746
538	22179	7188	1798	247932	340	4029	7165	1.398356	0.031254
566	32310	8295	3125	430893	368	7263	7798	1.488509	0.030294
567	47224	15081	4159	573511	530	8472	14984	1.506329	0.027954
595	32278	14026	2397	330488	601	5288	14753	1.596860	0.039190
596	45018	10280	4343	598834	587	5468	9314	1.420227	0.022610
629	28935	8225	2759	380417	315	6223	7949	1.534952	0.030157
630	53525	10385	5736	790945	677	6403	8844	1.498941	0.022510
663	43656	15249	3891	536545	490	6361	15438	1.610080	0.026285
664	47228	10579	4937	680766	370	5262	9521	1.528763	0.016837
697	53593	10233	6008	828376	629	8806	8655	1.560911	0.024725
698	28548	9161	2632	362852	421	5854	9112	1.580771	0.034567
721	29417	8445	2705	372912	275	4295	8182	1.486988	0.022042
722	89833	21577	9233	1273004	1031	11018	19875	1.540858	0.022148
735	25137	7527	1547	213331	384	4479	7369	1.016647	0.026401
736	135972	15607	11137	1535517	990	16510	9394	1.027220	0.013339
769	44527	10987	2915	401900	459	6353	10207	0.991579	0.018715

Session Spot Number	$^{206}Pb_m$	$^{207}Pb_m$	$^{235}U_m$	$^{238}U_m$	$N^{1/2}\sigma_{206Pbm}$	$N^{1/2}\sigma_{238Um}$	$^{206}Pb_{com}$ (Eqn. A4)	f_{206} (Eqn. A2a)	σ_{f206} (Eqn. A3a)
770	64776	11374	4931	679836	788	10172	9255	1.036835	0.019991
793	27729	7242	1841	253811	365	5754	6841	1.028920	0.026968
794	78376	31324	4358	600839	679	8760	32507	1.109178	0.018813
818	31482	6979	2578	355392	375	4780	6259	1.193090	0.021437
819	24994	7632	1866	257305	411	2936	7506	1.245834	0.024941
841	52075	10791	4577	631014	498	6931	9439	1.253208	0.018246
842	25216	7914	2101	289747	368	4861	7833	1.411440	0.031400
872	42368	8456	4158	573303	453	5305	7286	1.383793	0.019573
873	34467	8122	3511	484123	478	7100	7436	1.516537	0.030602
898	25198	7064	1495	206104	400	4253	6802	0.948709	0.024701
899	33965	9079	1978	272690	419	4936	8632	0.911483	0.019966
917	45858	10129	3093	426474	482	5749	9071	0.981674	0.016784
918	39234	7210	2728	376106	375	5795	5995	0.958145	0.017374
931	24394	7066	1533	211328	418	2937	6862	1.020694	0.022512
932	83588	25792	4806	662697	561	8105	25429	0.964857	0.013460
956	41315	9125	2876	396559	387	4484	8172	1.013162	0.014884
957	67856	14173	4997	688995	687	8687	12435	1.052691	0.017024
985	45443	13530	3384	466528	464	4935	13227	1.226237	0.018036
986	50846	10204	4372	602803	707	6272	8812	1.214353	0.021088
1014	37295	6975	3312	456684	515	4763	5846	1.229637	0.021281
1015	24270	6831	2005	276457	425	3735	6585	1.323724	0.029266
1048	22990	5842	2063	284423	402	4796	5476	1.375124	0.033383
1049	34044	6731	3265	450110	421	6285	5778	1.348391	0.025138
1052	58841	21408	4078	562283	521	5374	21846	1.286985	0.016775
1053	57158	12202	5519	760976	425	7836	10793	1.389803	0.017653
1086	26504	7913	2432	335386	439	5061	7741	1.513534	0.033924
1087	49152	21211	3451	475822	474	6017	22287	1.499781	0.023852
1110	39415	8507	4059	559689	513	6005	7555	1.487536	0.025078
1111	28908	8808	2715	374378	423	2826	8659	1.565586	0.025796
1124	18245	4255	1231	169732	281	3574	3883	1.000686	0.026105
1125	26716	5573	1933	266489	340	4757	4887	1.033750	0.022655
1153	30167	6332	2251	310357	300	5878	5566	1.068243	0.022855
1154	27541	5423	2237	308399	451	5034	4647	1.140650	0.026365
1182	36943	7469	2913	401651	580	3803	6470	1.116089	0.020453
1183	29505	5702	2540	350256	344	5911	4847	1.202839	0.024667
1211	34633	6036	2942	405653	299	5814	4893	1.154981	0.019333
1212	49351	7158	4378	603648	607	5954	5222	1.158308	0.018263
1245	24408	5261	2114	291504	361	2486	4670	1.250588	0.021361
1246	40181	6995	3607	497306	426	9237	5668	1.220121	0.026099
1279	34212	7877	2959	408019	498	6157	7156	1.276999	0.026768
1280	44859	8982	4368	602248	535	9519	7750	1.374238	0.027211

Notes: $\left(\frac{^{207}Pb_{com}}{^{206}Pb_{com}}\right)$ = 0.881984; $\left(\frac{^{207*}Pb_t}{^{235}U_t}\right)$ = 0.6753828; $\left(\frac{^{206*}Pb_t}{^{238}U_t}\right)$ = 0.0846772; fractionation factor for $\left(\frac{^{207*}Pb_t}{^{206*}Pb_t}\right)$ assumed = 1.

TABLE 12-A2. SELECTED COMMON PB CORRECTED AGES AND ERRORS BASED ON ISOTOPIC SUMS

Spot Name*	Session Spot No.	$(^{207}Pb_{com}/^{206}Pb_{com})_{unk}$	$f_{206}{}^{206}Pb_m$ (cps)	$f_{207}{}^{207}Pb_m$ (cps)	$^{206}Pb_{com}$ (cps)	$^{207}Pb_{com}$ (cps)	$^{235}U_m$ ($=^{238}U_m/137.88$) (cps)	$^{238}U_m$ (cps)	$^{206*}Pb/^{238}U_m$	$^{207*}Pb/^{235}U_m$
1	797	0.948112	391084	77041	48346	45838	9874	1361478	0.251740	3.159993
2	798	0.947694	480914	53939	11975	11348	13558	1869310	0.250862	3.141514
3	799	0.917173	68266	47455	50638	46443	1567	216042	0.081599	0.645420
5	801	0.972875	1565552	175322	13291	12930	37120	5118149	0.303286	4.374744
6	802	0.954928	1023888	153154	65410	62462	26132	3603112	0.266014	3.470502
8	804	0.960179	260379	47818	26012	24977	6137	846207	0.276961	3.721676
9	805	0.94381	135007	29291	20231	19094	3430	472928	0.242693	2.972755
10	806	0.917173	63516	45987	49275	45193	1461	201374	0.070722	0.543155
13	807	0.943642	766829	118924	59500	56146	21169	2918755	0.242339	2.965590
14	808	0.939486	862416	113607	45569	42812	25365	3497285	0.233566	2.791111
15	809	0.94435	287481	58640	38612	36463	7403	1020668	0.243829	2.995880
16	810	0.965544	143698	32127	20455	19750	3102	427770	0.288107	3.989515
17	811	0.946452	403148	55939	22868	21643	11110	1531835	0.248252	3.086939
18	812	0.943048	562326	111454	72216	68103	14744	2032932	0.241086	2.940255
20	813	0.94102	597257	73823	25308	23815	17517	2415254	0.236807	2.854801
21	814	0.93795	5263419	502893	59520	55827	163872	22594640	0.230316	2.728146
24	816	0.943989	136452	43712	36931	34862	2970	409438	0.243070	2.980409
25	817	0.951792	219886	48528	32705	31128	5232	721443	0.259454	3.325467
26	822	0.943307	261404	50444	31926	30116	6888	949698	0.241633	2.951291
27	823	0.957885	69992	28423	25170	24110	1194	164674	0.272183	3.610623
28	824	0.917173	67292	48523	51980	47675	1615	222673	0.068762	0.525311
29	825	0.974215	388664	62168	24405	23776	8632	1190183	0.306053	4.447606
32	827	0.917173	97146	45410	45603	41826	2452	338080	0.152459	1.461759
33	828	0.975005	321457	58875	28586	27872	6904	951855	0.307684	4.490938
36	830	0.945635	119338	39226	33315	31503	2531	348931	0.246534	3.051368
37	831	0.974293	501497	58346	6293	6131	11729	1617187	0.306213	4.451858
39	832	0.970222	510314	72817	23308	22614	11861	1635348	0.297799	4.232713
40	833	0.975517	342762	52839	18923	18460	7607	1048904	0.308740	4.519171
41	834	0.917173	67314	48866	52368	48030	1501	206950	0.072222	0.556937
42	835	0.954906	140602	22304	10463	9992	3549	489301	0.265968	3.469478
44	836	0.947101	158999	70774	65821	62339	2707	373287	0.249615	3.115351
45	837	0.969375	601679	86408	28469	27597	14043	1936225	0.296045	4.187972
49	839	0.974758	2075805	248771	33746	32894	48215	6647871	0.307175	4.477387
50	840	0.947671	413797	80346	49913	47301	10522	1450816	0.250814	3.140490
51	845	0.982443	510786	64729	9616	9448	11253	1551555	0.323011	4.912574
52	846	0.917173	72949	51346	54875	50330	1772	244336	0.073970	0.573123
53	847	0.917173	77745	58272	62596	57411	1410	194385	0.077932	0.610331
55	848	0.93953	88268	57427	58364	54835	928	127981	0.233658	2.792916
56	849	0.946657	317683	57513	33664	31868	8283	1142086	0.248684	3.095945
58	850	0.917173	65593	49749	53496	49065	1148	158261	0.076440	0.596226
59	851	0.917173	116770	33188	31035	28464	9320	1285030	0.066719	0.506894
60	852	0.949614	226634	40868	23383	22205	5783	797400	0.254892	3.226948
61	853	0.937766	222117	82873	74901	70239	4644	640277	0.229926	2.720657
62	854	0.937304	732614	194359	154574	144883	18311	2524761	0.228948	2.701911
63	855	0.966858	99603	36183	30156	29157	1732	238784	0.290833	4.056918
64	856	0.946375	81184	44033	42880	40580	1120	154398	0.248091	3.083600
65	857	0.917173	66290	49625	53317	48901	1320	182038	0.071264	0.548118
66	858	0.945374	327544	74935	53259	50349	8087	1115052	0.245985	3.040046
68	859	0.937765	149453	44683	37393	35066	3535	487375	0.229924	2.720617
69	860	0.917173	63016	48618	52381	48042	1288	177555	0.059896	0.446740
70	861	0.949939	258255	93343	81108	77047	5027	693135	0.255574	3.241546
71	862	0.952138	181197	54030	43252	41182	3845	530192	0.260179	3.341303
72	863	0.917173	62293	49512	53478	49049	1311	180762	0.048763	0.352928

Spot Name*	Session Spot No.	$(^{207}Pb_{com}/^{206}Pb_{com})_{unk}$	$f_{206}{}^{206}Pb_m$ (cps)	$f_{207}{}^{207}Pb_m$ (cps)	$^{206}Pb_{com}$ (cps)	$^{207}Pb_{com}$ (cps)	$^{235}U_m$ (=$^{238}U_m$/*137.88*) (cps)	$^{238}U_m$ (cps)	$^{206*}Pb/^{238}U_m$	$^{207*}Pb/^{235}U_m$
73	864	0.917173	594007	94414	61304	56227	23608	3255004	0.163657	1.617611
74	865	0.917173	485782	68450	47587	43645	41453	5715478	0.076668	0.598379
75	866	0.967239	644970	101353	41534	40173	15008	2069237	0.291623	4.076594
76	867	1.017431	36040	21106	18433	18755	323	44602	0.394754	7.267598
77	868	0.940707	251604	42655	24250	22812	6983	962767	0.236146	2.841737
78	869	0.940667	240173	74697	62971	59235	5444	750654	0.236063	2.840095
79	870	0.938696	263023	70742	56367	52912	6463	891156	0.231896	2.758649
80	871	0.964634	395379	52515	15043	14511	9638	1328819	0.286221	3.943310
83	877	0.95596	279674	46711	23344	22316	6933	955859	0.268168	3.519011
85	878	0.947919	840143	98554	25848	24501	23498	3239879	0.251335	3.151463
86	879	0.957387	97555	16735	8562	8197	2380	328214	0.271145	3.586785
88	880	0.985355	134854	37446	25571	25197	2409	332166	0.328999	5.084534
91	881	0.955795	886238	120751	42388	40514	22852	3150782	0.267823	3.511209
92	882	1.105442	4400	2035	1214	1342	40	5461	0.583436	17.501804
93	883	0.94152	73705	43873	43814	41252	911	125666	0.237863	2.875736
95	884	0.946052	88835	24987	19851	18780	2022	278825	0.247411	3.069494
96	885	0.917173	70968	54043	58170	53352	1566	215946	0.059269	0.441310
97	886	0.941529	1003664	373074	333861	314339	20421	2815698	0.237882	2.876109
98	887	0.942707	265244	61038	44031	41509	6675	920316	0.240366	2.925776
99	888	0.947861	242491	34740	14815	14042	6573	906311	0.251212	3.148865
100	889	0.917173	73362	53865	57826	53036	2064	284594	0.054590	0.401366
102	890	0.917173	66275	50531	54348	49847	1061	146279	0.081534	0.644795
103	891	0.982744	50663	25468	22780	22387	625	86156	0.323630	4.930162
104	892	0.953612	93289	15963	8377	7988	2339	322535	0.263263	3.409197
105	893	0.917173	60237	48095	51948	47645	988	136210	0.060858	0.455098
107	894	0.947918	174763	48204	37703	35740	3955	545329	0.251334	3.151431
108	895	0.917173	59788	46780	50465	46285	1281	176652	0.052774	0.386122
110	897	0.917173	57866	45515	49091	45025	889	122630	0.071553	0.550775
11	935	0.917173	17916	7960	8010	7347	656	90499	0.109449	0.933643
12	936	0.947595	114158	41776	36662	34741	2242	309173	0.250655	3.137162
19	937	0.940519	544509	80910	39185	36854	15546	2143475	0.235750	2.833930
23	938	0.96091	115426	42888	36606	35175	2053	283036	0.278482	3.757501
30	939	0.917173	54254	35987	38194	35031	1220	168281	0.095438	0.783743
34	940	0.945397	185199	44602	32720	30933	4495	619751	0.246033	3.041050
38	941	0.945978	232553	49935	33899	32068	5827	803434	0.247255	3.066278
43	942	0.946505	285896	95135	80981	76649	5984	825062	0.248363	3.089266
48	944	0.94473	108536	35290	29924	28270	2331	321352	0.244629	3.012230
54	945	0.945644	81351	33278	30349	28699	1500	206859	0.246552	3.051744
82	948	0.917173	61463	41567	44242	40578	1519	209384	0.082244	0.651670
84	949	0.960215	419008	53884	15115	14513	10574	1457914	0.277035	3.723415
87	950	0.950831	485626	57087	14199	13501	13281	1831186	0.257443	3.281809
89	951	0.94952	90649	21349	15191	14425	2149	296267	0.254693	3.222707
90	952	0.95125	599080	84844	34155	32490	15861	2186935	0.258318	3.300761
94	953	0.917173	51728	34444	36455	33436	831	114544	0.133335	1.213637
101	954	0.944907	192060	35578	21517	20332	5048	696083	0.245004	3.019896
106	955	0.959545	29368	13462	12303	11805	449	61909	0.275642	3.690799

* All spot names are preceded by the letters 1711D1

TABLE 12-A2. SELECTED COMMON PB CORRECTED AGES AND ERRORS BASED ON ISOTOPIC SUMS (CONTINUED)

Spot Name*	t $^{206*}Pb/^{238}Um$ (Ma)	t $^{207*}Pb/^{235}Um$ (Ma)	N $1/2\sigma$ ^{206}Pbm (cps)	N $1/2\sigma$ ^{207}Pbm (cps)	N $1/2\sigma$ ^{238}Um (cps)	$-\sigma_{t206Pb}$ (Eq. A7a) (Ma)	$-\sigma_{t207Pb}$ (Eq. A7b) (Ma)	$-\sigma_{t238U}$ (Eq. A7c) (Ma)	$+\sigma_{t206Pb}$ (Eq. A7d) (Ma)	$+\sigma_{t207Pb}$ (Eq. A7e) (Ma)	$+\sigma_{t238U}$ (Eq. A7f) (Ma)	t_{tPbcom} (Eq. A5) (Ma)	$-\sigma_{tPbcom}$ (Eq. A8a) (Ma)	$+\sigma_{tPbcom}$ (Eqn. A8b)
1	1447.4	1447.4	2061	845	12259	61.6	-26.7	-78.7	-61.6	26.6	70.7	1447.4	75.5	61.6
2	1442.9	1442.9	2275	627	16024	49.7	-14.5	-74.4	-49.7	14.5	67.2	1442.9	68.8	49.7
3	505.7	505.7	793	549	4361	159.2	-118.7	-66.8	-157.0	120.0	52.8	505.7	131.1	157.0
5	1707.6	1707.6	5614	1068	23438	45.2	-8.9	-46.4	-45.3	8.8	43.8	1707.6	44.7	45.3
6	1520.5	1520.5	2405	553	23871	27.6	-6.6	-60.0	-27.6	6.6	55.5	1520.5	55.9	27.6
8	1576.0	1576.0	1004	381	4070	49.3	-19.5	-44.7	-49.4	19.5	42.2	1576.0	46.5	49.4
9	1400.7	1400.7	1185	388	7755	104.8	-36.4	-145.2	-104.7	36.4	119.5	1400.7	125.0	104.7
10	440.5	440.5	358	444	4819	78.9	-105.8	-70.9	-78.4	106.9	53.6	440.5	119.6	78.4
13	1398.8	1398.8	2948	620	13795	42.5	-9.5	-38.8	-42.5	9.5	36.7	1398.9	37.9	42.5
14	1353.2	1353.2	2172	811	19766	26.2	-10.4	-45.1	-26.2	10.4	42.2	1353.2	43.5	26.2
15	1406.6	1406.6	1715	482	7471	71.1	-21.2	-61.4	-71.1	21.2	56.3	1406.6	60.2	71.1
16	1632.1	1632.1	1049	483	6852	103.9	-49.6	-166.5	-104.3	49.5	136.9	1632.1	145.6	104.3
17	1429.5	1429.5	1502	504	13071	41.8	-14.8	-73.4	-41.8	14.8	66.3	1429.5	67.9	41.8
18	1392.3	1392.3	2223	1074	21193	46.8	-24.0	-88.3	-46.8	24.0	78.0	1392.3	81.6	46.8
20	1370.1	1370.1	1601	617	18996	28.5	-11.7	-64.5	-28.5	11.7	58.8	1370.1	59.9	28.5
21	1336.2	1336.2	17262	1938	182471	33.0	-3.9	-64.6	-32.9	3.9	58.7	1336.2	58.9	32.9
24	1402.6	1402.6	688	402	6302	72.9	-45.1	-135.6	-72.9	45.1	113.0	1402.6	121.6	72.9
25	1487.0	1487.0	1172	439	9664	70.5	-27.8	-123.8	-70.5	27.8	105.5	1487.1	109.1	70.5
26	1395.2	1395.2	1066	498	10478	49.7	-24.6	-94.0	-49.7	24.6	82.5	1395.2	86.1	49.7
27	1551.9	1551.9	690	335	4209	185.6	-94.3	-269.0	-186.4	94.1	197.2	1551.9	218.5	186.4
28	428.7	428.7	569	599	4856	121.0	-137.1	-62.0	-119.7	138.9	48.1	428.7	146.9	119.7
29	1721.3	1721.3	1260	625	8994	46.6	-23.8	-77.5	-46.7	23.7	70.7	1721.3	74.6	46.7
32	914.7	914.7	824	571	4439	112.0	-84.2	-74.2	-111.3	84.6	63.8	914.7	105.9	111.3
33	1729.3	1729.3	1210	630	10823	57.3	-30.6	-122.1	-57.5	30.6	106.1	1729.3	110.4	57.5
36	1420.6	1420.6	873	470	3561	113.5	-64.7	-88.1	-113.5	64.7	78.1	1420.6	101.4	113.5
37	1722.0	1722.0	1693	465	22199	47.6	-13.4	-149.1	-47.7	13.4	125.8	1722.1	126.5	47.7
39	1680.4	1680.4	2416	594	19411	67.3	-17.1	-123.9	-67.5	17.1	107.1	1680.4	108.4	67.5
40	1734.5	1734.5	1130	409	8308	48.6	-18.1	-82.1	-48.7	18.1	74.6	1734.5	76.7	48.7
41	449.5	449.5	618	357	4390	145.9	-90.8	-62.9	-144.0	91.5	49.2	449.5	103.9	144.0
42	1520.3	1520.3	1138	386	9580	107.0	-38.0	-193.2	-107.2	38.0	152.6	1520.3	157.2	107.2
44	1436.5	1436.5	691	785	6075	86.8	-104.1	-150.2	-86.8	104.1	123.4	1436.5	161.4	86.8
45	1671.7	1671.7	4105	732	20415	98.1	-18.1	-108.4	-98.5	18.1	95.3	1671.7	97.0	98.5
49	1726.8	1726.8	6652	1616	51061	46.6	-11.6	-80.3	-46.8	11.6	73.1	1726.8	74.0	46.8
50	1442.7	1442.7	2063	716	17635	66.5	-24.4	-108.0	-66.5	24.4	93.4	1442.7	96.6	66.5
51	1804.4	1804.4	1703	623	11850	52.2	-19.5	-83.9	-52.4	19.5	76.2	1804.4	78.7	52.4
52	460.0	460.0	948	472	5947	193.8	-103.8	-74.2	-190.5	104.7	56.1	460.0	118.8	190.5
53	483.8	483.8	645	521	2066	170.4	-148.1	-32.2	-167.9	150.1	28.4	483.8	152.7	167.9
55	1353.6	1353.6	744	536	2561	275.9	-210.8	-172.4	-275.4	211.1	136.5	1353.6	251.4	275.4
56	1431.7	1431.7	1922	711	15024	80.9	-31.6	-116.7	-80.9	31.6	99.8	1431.7	104.7	80.9
58	474.8	474.8	450	649	4002	143.1	-221.8	-80.0	-141.3	226.2	59.8	474.8	234.0	141.3
59	416.4	416.4	889	430	9913	35.5	-18.6	-19.5	-35.4	18.7	17.8	416.4	25.8	35.4
60	1463.7	1463.7	853	429	9701	51.8	-27.4	-109.7	-51.8	27.4	94.9	1463.7	98.8	51.8
61	1334.1	1334.1	1239	684	6445	94.4	-55.5	-81.4	-94.3	55.5	72.3	1334.1	91.2	94.3
62	1329.0	1329.0	1306	1021	19447	25.3	-21.1	-61.1	-25.3	21.1	55.8	1329.0	59.7	25.3
63	1645.7	1645.7	655	323	4003	133.7	-68.5	-176.8	-134.4	68.3	144.0	1645.7	159.4	134.4
64	1428.6	1428.6	488	529	3077	155.0	-177.6	-184.5	-155.0	177.5	145.5	1428.6	229.5	155.0
65	443.8	443.8	560	388	3209	158.7	-118.5	-49.6	-156.5	119.7	40.6	443.8	126.4	156.5
66	1417.7	1417.7	1080	761	10871	48.5	-36.1	-85.0	-48.5	36.1	75.6	1417.7	83.8	48.5
68	1334.1	1334.1	1075	414	6376	109.4	-44.9	-107.8	-109.3	44.9	92.4	1334.1	102.8	109.3
69	375.0	375.0	631	381	3197	186.4	-120.8	-43.1	-183.2	122.2	35.0	375.0	127.1	183.2
70	1467.2	1467.2	1234	587	8640	87.2	-43.7	-111.2	-87.3	43.7	96.0	1467.2	105.5	87.3
71	1490.8	1490.8	1285	367	8070	119.0	-35.7	-140.5	-119.2	35.7	117.4	1490.8	122.7	119.2
72	306.9	306.9	499	419	2959	146.5	-132.4	-31.8	-144.5	134.1	26.4	306.9	136.7	144.5
73	977.1	977.1	2777	684	114661	43.6	-11.7	-246.8	-43.5	11.7	163.2	977.1	163.6	43.5
74	476.2	476.2	2014	694	28534	18.7	-7.0	-14.2	-18.7	7.0	13.4	476.2	15.1	18.7
75	1649.6	1649.6	2589	428	14141	62.1	-10.6	-66.6	-62.2	10.6	61.4	1649.6	62.3	62.2
76	2144.8	2144.8	373	264	2210	419.6	-307.1	-2748.3	-449.8	293.2	473.8	2144.8	557.2	449.8
77	1366.6	1366.6	1250	596	11104	66.0	-33.4	-96.5	-66.0	33.4	84.2	1366.6	90.6	66.0

Spot Name*	$t_{^{206*}Pb/^{238}Um}$ (Ma)	$t_{^{207*}Pb/^{235}Um}$ (Ma)	$N\ 1/2\sigma\ ^{206}Pbm$ (cps)	$N\ 1/2\sigma\ ^{207}Pbm$ (cps)	$N\ 1/2\sigma\ ^{238}Um$ (cps)	$-\sigma_{t206Pb}$ (Eq. A7a) (Ma)	$-\sigma_{t207Pb}$ (Eq. A7b) (Ma)	$-\sigma_{t238U}$ (Eq. A7c) (Ma)	$+\sigma_{t206Pb}$ (Eq. A7d) (Ma)	$+\sigma_{t207Pb}$ (Eq. A7e) (Ma)	$+\sigma_{t238U}$ (Eq. A7f) (Ma)	t_{tPbcom} (Eq. A5) (Ma)	$-\sigma_{tPbcom}$ (Eq. A8a) (Ma)	$+\sigma_{tPbcom}$ (Eqn. A8b)
78	1366.2	1366.2	1070	567	5678	71.6	-40.3	-60.8	-71.5	40.3	55.7	1366.2	68.7	71.5
79	1344.4	1344.4	871	584	9112	50.0	-35.6	-83.4	-50.0	35.7	74.0	1344.4	82.1	50.0
80	1622.6	1622.6	2098	433	8282	79.5	-17.0	-59.5	-79.7	17.0	55.2	1622.6	57.7	79.7
83	1531.5	1531.5	902	370	8891	49.1	-21.1	-86.4	-49.1	21.1	77.3	1531.5	80.1	49.1
85	1445.4	1445.4	2261	442	17959	35.9	-7.4	-46.6	-35.9	7.4	43.7	1445.4	44.3	35.9
86	1546.6	1546.6	805	231	5951	126.3	-38.0	-177.5	-126.6	37.9	143.0	1546.6	148.0	126.6
88	1833.5	1833.5	794	451	6099	123.9	-71.8	-217.8	-125.0	71.5	173.1	1833.5	187.3	125.0
91	1529.7	1529.7	2749	516	23933	45.2	-8.9	-68.6	-45.2	8.9	62.8	1529.7	63.4	45.2
92	2962.8	2962.8	296	97	1686	2937.7	-846.9	2962.8	-2323.7	920.9	1908.1	2962.8	1481.4	798.6
93	1375.6	1375.6	582	419	3113	242.1	-184.9	-224.1	-241.8	185.1	167.6	1375.6	249.7	241.8
95	1425.1	1425.1	714	285	5812	135.8	-57.2	-193.7	-135.9	57.2	151.1	1425.1	161.5	135.9
96	371.2	371.2	478	417	4819	127.7	-120.1	-56.2	-126.1	121.4	43.1	371.2	128.9	126.1
97	1375.7	1375.7	2263	1593	10118	42.9	-32.1	-28.8	-42.9	32.1	27.6	1375.7	42.3	42.9
98	1388.6	1388.6	1092	489	10281	63.5	-30.2	-94.8	-63.4	30.2	83.1	1388.6	88.4	63.4
99	1444.7	1444.7	1023	303	11039	60.5	-18.9	-108.4	-60.5	18.9	93.8	1444.7	95.6	60.5
100	342.6	342.6	486	432	4822	98.2	-94.5	-37.5	-97.3	95.3	30.7	342.6	100.1	97.3
102	505.3	505.3	518	587	3120	202.1	-244.9	-71.0	-198.6	250.2	55.4	505.3	252.6	198.6
103	1807.4	1807.4	391	328	2588	241.0	-208.5	-383.2	-245.0	205.6	262.3	1807.4	333.3	245.0
104	1506.5	1506.5	554	312	5436	92.8	-54.9	-161.6	-93.0	54.8	132.0	1506.5	143.0	93.0
105	380.8	380.8	478	415	3352	204.1	-190.0	-63.5	-200.3	193.4	47.6	380.8	190.4	200.3
107	1445.3	1445.4	959	528	5727	95.7	-55.6	-92.5	-95.7	55.6	81.6	1445.4	98.8	95.7
108	331.5	331.5	671	488	4300	223.7	-173.8	-54.7	-218.9	176.8	41.1	331.5	165.8	218.9
110	445.5	445.5	485	317	2851	228.1	-159.5	-68.2	-223.5	161.8	52.2	445.5	170.0	223.5
11	669.5	669.5	344	174	2771	143.9	-78.9	-143.0	-142.3	79.4	100.1	669.6	127.7	142.3
12	1441.9	1441.9	1547	461	18107	182.5	-57.4	-753.0	-182.6	57.4	359.0	1441.9	363.6	182.6
19	1364.6	1364.6	2489	699	18676	42.6	-12.7	-71.5	-42.5	12.7	64.5	1364.6	65.8	42.5
23	1583.7	1583.7	946	354	4601	122.5	-47.8	-163.8	-122.9	47.7	134.5	1583.7	142.7	122.9
30	587.6	587.6	789	494	3077	181.6	-122.3	-69.2	-179.0	123.6	56.0	587.6	135.6	179.0
34	1418.0	1418.0	1171	581	8710	69.8	-36.7	-124.1	-69.8	36.7	105.1	1418.0	111.3	69.8
38	1424.3	1424.3	1561	399	9930	72.0	-19.5	-108.5	-72.0	19.5	93.7	1424.3	95.7	72.0
43	1430.0	1430.0	1358	790	10105	61.2	-37.6	-107.9	-61.2	37.6	93.3	1430.0	100.6	61.2
48	1410.7	1410.7	1163	584	6132	135.5	-72.0	-173.3	-135.5	72.0	138.1	1410.7	155.8	135.5
54	1420.7	1420.7	672	424	4428	122.0	-81.5	-199.1	-122.0	81.5	154.2	1420.7	174.4	122.0
82	509.5	509.5	448	517	3717	85.5	-106.6	-58.2	-84.9	107.6	47.4	509.5	117.5	84.9
84	1576.4	1576.4	2175	517	16735	55.8	-13.8	-109.8	-55.9	13.8	95.7	1576.4	96.7	55.9
87	1476.7	1476.7	2342	975	21381	48.0	-21.1	-104.3	-48.1	21.0	90.9	1476.8	93.3	48.1
89	1462.6	1462.6	895	382	5114	113.9	-51.2	-158.3	-114.0	51.2	129.2	1462.6	138.9	114.0
90	1481.2	1481.2	2548	504	18446	44.0	-9.2	-74.1	-44.1	9.2	67.1	1481.2	67.7	44.1
94	806.9	806.9	803	422	3011	280.0	-158.2	-143.1	-275.0	159.8	105.4	806.9	191.4	275.0
101	1412.7	1412.7	1397	474	8905	77.5	-27.8	-111.6	-77.5	27.8	95.9	1412.7	99.9	77.5
106	1569.4	1569.4	301	250	2526	187.7	-163.4	-490.5	-188.6	162.8	295.3	1569.4	337.2	188.6

* All spot names are preceded by the letters 1711D1